

Regularisation in Nonperturbative Extensions of Effective Field Theory

Curtis D. Abell,¹ Derek B. Leinweber,¹ Anthony W. Thomas,¹ and Jia-Jun Wu²

¹*Special Research Centre for the Subatomic Structure of Matter (CSSM),
Department of Physics, University of Adelaide, Adelaide, South Australia 5005, Australia*

²*School of Physical Sciences, University of Chinese Academy of
Sciences (UCAS), Beijing 100049, China*

The process of renormalisation in nonperturbative Hamiltonian Effective Field Theory (HEFT) is examined in the Δ -resonance scattering channel. As an extension of effective field theory, HEFT provides a bridge between the infinite-volume scattering data of experiment and the finite-volume spectrum of energy eigenstates in lattice QCD. The extent to which the established features of finite-range regularisation survive in HEFT is examined. While phase shifts withstand large variations in the renormalisation scheme, inelasticities in the two-channel, πN , $\pi\Delta$ case do not. The regularisation-scheme dependence of the Hamiltonian energy eigenvectors is explored to ascertain the conditions under which these eigenvectors provide physically relevant insight into the basis-state composition of the finite volume states. As in perturbative effective field theory, variation in the regularisation scale is compensated by variation in the residual series of short-distance counter terms. Unphysical regulators lead to large corrections in the residual series, resulting in an unphysical Hamiltonian and its associated eigenvectors. Physically relevant regulators are required to maintain convergence in the residual series expansion of the bare basis-state mass; with correct physics contained within the interactions of the Hamiltonian, physical insight can flow from the eigenvectors. A scheme is established for the prediction of the quark-mass dependence of the finite-volume Δ spectrum, to be observed in future lattice QCD simulations.

I. INTRODUCTION

The calculation of scattering observables from first principles in lattice QCD simulations is facilitated by an understanding of the impact of the lattice finite volume on the spectrum of observed states. The most prominent method for converting quantities obtained through lattice QCD into physical scattering observables is that developed by Lüscher [1–3]. With only a single open scattering channel, Lüscher’s method can be used to calculate a scattering phase shift from a single eigenstate generated on a finite volume through a relatively straight-forward process.

While this process has been generalised to cases such as multiple scattering channels [4–10], and three-body systems [11–13], it requires parametrisation of the scattering observables and becomes significantly more complicated. Through increases in computational power and algorithmic advances, lattice QCD is now able to consider physical quark masses, yielding, for example, results for the lowest-lying resonance, the $\Delta(1232)$ [14–16].

Hamiltonian Effective Field Theory (HEFT) also allows for the conversion between lattice QCD quantities and physical quantities, and may have advantages for systems involving multiple scattering channels. Here the parametrisation is performed in constructing the Hamiltonian describing the scattering process. Single and non-interacting multi-particle basis states are then mixed in solving the Hamiltonian system and insight into the composition of the states is contained in the energy eigenvectors of the Hamiltonian. On multiple occasions, HEFT has been shown to produce results equivalent to Lüscher’s method [17, 18] up to exponentially suppressed terms in the lattice size L . However insights into the composition of the states is unique to HEFT.

To ensure the residual series contributions are small, one must select phenomenologically motivated regularisation schemes to ensure the physics is contained within the Hamil-

tonian. With this constraint, the physics of the dynamics is contained within the Hamiltonian, and the energy eigenvectors contain physically relevant insight into the structure of resonances.

In chiral perturbation theory (χ PT), working within the power-counting regime (PCR) where higher order terms of the chiral expansion make a negligible contribution, the independence of results on the regularisation method is well understood. Consider, the finite-range regularisation (FRR) formalism where a momentum regulator, governed by Λ , is introduced into loop integrals to suppress the effective-field contributions at large momenta. Each Λ -dependent term in the PCR is accompanied by a (Λ -dependent) counter term constrained by phenomenology. In this way the regulator cannot have any impact, provided one works within the PCR [19–21].

In a nonperturbative extension of effective field theory (EFT), the process of renormalisation has a significant impact on the results. The couplings between the basis states are significantly renormalised, introducing a new degree of influence in the calculations. We will illustrate how the role of a single particle basis state can be exchanged for two-particle states within the Hamiltonian, provided the regulator allows strong short-distance attractive interactions. We also demonstrate the regularisation independence of the finite-volume eigenstate energies in accord with the expectations of EFT in the PCR.

However, upon examining the quark-mass dependence of the nonperturbative EFT, one discovers a transfer of physics from the Hamiltonian to the residual series expansion of counter-terms as the regulator parameter, Λ , becomes large. When the residual series contributions are large, the physics contained in the Hamiltonian is unphysical and the Hamiltonian’s ability to predict the quark-mass dependence of the energy eigenvalues is poor.

In this work we take the $\Delta(1232)$ as a case study to explore the process of regularisation of the nonperturbative extension of effective field theory, HEFT. As the energy eigenvectors

describing the composition of the states are renormalisation dependent, our aim is to understand the extent to which one can obtain insight into the structure of a resonance through the application of HEFT.

We commence our report with a brief review of the FRR formalism in perturbation theory in Sec. II. Our aim here is to present the residual series expansion and connect its role to HEFT. In Sec. III we present the details of the HEFT approach. This is followed in Sec. IV by an analysis of renormalisation in the single πN -channel calculation of the πN phase shifts and the corresponding finite-volume lattice energy levels. In Sec. V the analysis is extended to the two-channel case, where the $\pi\Delta$ coupled channel is included, giving access to somewhat higher energies. We finish with an outline of the conclusions in Sec. VI.

II. FINITE-RANGE REGULARISATION IN PERTURBATION THEORY

The Δ resonance has the formal quark-mass expansion ($m_q \propto m_\pi^2$, [22])

$$M_\Delta = \{a_0^\Lambda + a_2^\Lambda m_\pi^2 + a_4^\Lambda m_\pi^4 + \dots\} + \Sigma_{\pi\Delta}(m_\pi^2, \Lambda) + \Sigma_{\pi N}(m_\pi^2, \Lambda) + \Sigma_{t\Delta}(m_\pi^2, \Lambda). \quad (1)$$

The leading terms in $\{\dots\}$ are referred to as the residual series expansion and it plays a central role in the process of renormalisation. This is indicated by the appearance of the regulator parameter, Λ , as a superscript on the coefficients of the expansion. The residual series is vital to maintaining model independence. The quantities $\Sigma(m_\pi^2, \Lambda)$ contain pion loop integrals for the Δ resonance with intermediate states as described by the subscripts, where a subscript t denotes a tadpole term. The loop integrals are regulated by the parameter Λ , which can appear in a dipole or exponential regulator or as a momentum cutoff in a theta function, etc. These loop integrals generate the leading and next-to-leading non-analytic quark-mass terms for the Δ self energy. They have model-independent coefficients with known values.

The integrals can be evaluated analytically. For example, explicit forms for a sharp cutoff regulator are reported in Ref. [23]. To proceed with the process of renormalisation, one then expands the integral results about the chiral limit [24]. Working in the heavy-baryon limit for simplicity of presentation, one observes an analytic polynomial in m_π^2 and nonanalytic terms

$$\Sigma_{\pi\Delta} = b_0^\Delta \Lambda^3 + b_2^\Delta \Lambda m_\pi^2 + \chi_{\pi\Delta} m_\pi^3 + b_4^\Delta \frac{m_\pi^4}{\Lambda} + \dots, \quad (2)$$

$$\Sigma_{\pi N} = b_0^N \Lambda^3 + b_2^N \Lambda m_\pi^2 + \chi_{\pi N} \frac{m_\pi^4}{\delta M} \log m_\pi + b_4^N \frac{m_\pi^4}{\Lambda} + \dots, \quad (3)$$

$$\Sigma_{t\Delta} = b_2^t \Lambda^2 m_\pi^2 + c_2 \chi_{t\Delta} m_\pi^4 \log m_\pi + b_4^t m_\pi^4 + \dots. \quad (4)$$

Here δM is the Δ - N mass splitting in the chiral limit, $\chi_{\pi\Delta}$, $\chi_{\pi N}$, and $\chi_{t\Delta}$ denote the model independent chiral coefficients of the terms that are nonanalytic in the quark mass, and c_2 is a renormalised low-energy coefficient, discussed in the

following. The regulator dependence of the terms polynomial in m_π^2 is explicit.

The process of renormalisation in FRR χ EFT proceeds by combining the renormalisation-scheme dependent coefficients to provide the physical low energy coefficients, denoted as c_i . The Δ energy expansion has the form [24]

$$M_\Delta = c_0 + c_2 m_\pi^2 + \chi_{\pi\Delta} m_\pi^3 + c_4 m_\pi^4 + \left(\frac{\chi_{\pi N}}{\delta M} + c_2 \chi_{t\Delta}\right) m_\pi^4 \log m_\pi + \dots. \quad (5)$$

with the coefficients, c_i , given by

$$c_0 = a_0^\Lambda + b_0^\Delta \Lambda^3 + b_0^N \Lambda^3, \quad (6a)$$

$$c_2 = a_2^\Lambda + b_2^\Delta \Lambda + b_2^N \Lambda + b_2^t \Lambda^2, \quad (6b)$$

$$c_4 = a_4^\Lambda + \frac{b_4^\Delta}{\Lambda} + \frac{b_4^N}{\Lambda} + b_4^t, \text{ etc.} \quad (6c)$$

Strategies for implementing these formal relations in practice are presented in Ref. [24].

The essential point is that for a given regulator, one has complete freedom in the residual series coefficients, a_i^Λ , to address and remove any dependence on the choice of regulator. In this way, the coefficients c_i are scheme independent quantities. In the power-counting regime, FRR EFT is not a model.

The value of c_0 describes the Δ resonance in the chiral limit, and c_2 is related to the sigma term of explicit chiral symmetry breaking. The nonanalytic terms m_π^3 and $m_\pi^4 \log m_\pi$ have known, model-independent coefficients denoted by $\chi_{\pi N}$, $\chi_{\pi\Delta}$ and $\chi_{t\Delta}$. In practice, the coefficients, a_i^Λ , are determined by fitting to lattice QCD results.

The value of Λ determines the origin of the physics contributing to the renormalised coefficients, c_i . For small $\Lambda \sim 1$ GeV, the regulated loop integrals do not contain significant short-distance physics and can be associated with pion-cloud contributions. By preventing large momenta from flowing through the effective-field propagators, one avoids large errors that need to be rectified in the residual series.

The residual series coefficients are short-distance-related quantities directly tied to the cutoff as illustrated in Eqs. (6). The contributions are associated with a bare-baryon core contribution. A phenomenologically-motivated value for Λ will leave only small corrections to be contained within the residual series expansion.

Studies of renormalisation in FRR chiral effective field theory have shown the functional form of the cutoff to be unimportant [19–21]. By observing the flow of low-energy coefficients as a functions of the regulator parameter, Λ , [24–27], the scale of the dipole-regulator parameter was determined, $\Lambda \sim 1$ GeV. The phenomenologically motivated value of 0.8 GeV is associated with the induced pseudoscalar form factor of the nucleon [28], the source of the pion cloud. Values varying by ± 0.2 GeV are typically considered to explore alternative resummations of the expansion and inform estimates of the systematic error.

The key advantage of FRR for the extrapolation of lattice QCD results is that it provides a mechanism to exactly preserve the leading nonanalytic terms of chiral perturbation

theory, including the values of the model-independent coefficients of the nonanalytic terms, while addressing quark masses beyond the PCR. This contrasts other popular approaches that draw on the nonanalytic terms of the expansion, but relegate the model-independent coefficients of these terms to fit parameters. In the absence of FRR, the fit parameters of the nonanalytic terms may differ significantly from the known results of chiral perturbation theory and the extrapolation does not correctly incorporate the known leading nonanalytic behaviour. In contrast, while FRR develops a model dependence in how the chiral expansion sums to zero outside the PCR, it does preserve the correct leading and next-to-leading nonanalytic behaviour of QCD.

In returning our attention to HEFT, it is important to consider where the physics lies in the calculation. If one makes a poor choice for the regulator, short distance physics will not be correctly included in the loop integrals, and the coefficients, a_i^Λ , will need to be large in magnitude to ensure the renormalised coefficients take their correct physical values. In this case one would need to acknowledge that there is a significant role for the bare-baryon core contribution. Moreover, one might be concerned that the Hamiltonian theory is missing important physics that is put in by hand via the residual-series coefficients. In this case, intuition obtained from the Hamiltonian theory may have relatively poor value.

On the other hand, a good choice for the regulator can allow the residual series coefficients to become small at higher orders, presenting the possibility that the first two or three terms of the residual series are sufficient to describe the results from lattice QCD. Moreover, the Hamiltonian itself contains the correct physics such that insight into the structure of the states obtained from the energy eigenvectors of the theory is more robust.

Finally, we note that when working at a fixed pion mass such as the physical pion mass, the residual series of Eq. (1) sums to a single coefficient. We will refer to this as the bare-baryon mass, $m_\Delta^{(0)}$, and associate it with the bare-baryon basis state.

III. HAMILTONIAN FRAMEWORK

A. Hamiltonian Model

In the rest frame, the Hamiltonian for an interacting system can be represented by the form

$$H = H_0 + H_I, \quad (7)$$

where H_0 is the free, non-interacting Hamiltonian, and H_I is the interaction Hamiltonian. In the HEFT formalism we allow for a single-particle bare-baryon basis state $|B_0\rangle$, which may be thought of as a quark model state (a state in the P -space in the notation of Ref. [29]). With coupled two-particle channels

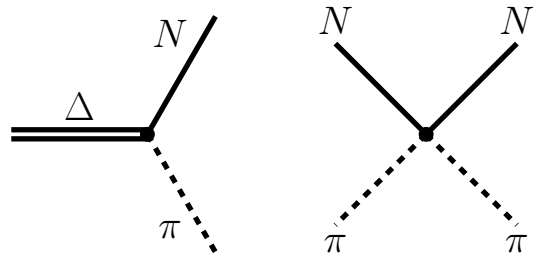


FIG. 1. Self-energy (left) and two-particle interaction (right) contributions to the Δ mass.

$|\alpha\rangle$, such as πN and $\pi\Delta$, H_0 can be expressed as

$$H_0 = |B_0\rangle m_{B_0} \langle B_0| + \sum_{\alpha} \int d^3k |\alpha(\mathbf{k})\rangle \left[\sqrt{m_{\alpha_B}^2 + k^2} + \sqrt{m_{\alpha_M}^2 + k^2} \right] \langle \alpha(\mathbf{k})|, \quad (8)$$

where m_{α_B} and m_{α_M} are the baryon and meson masses respectively in channel α , and m_{B_0} is the mass of the bare basis state. In general, H_I is governed by two types of interactions, examples of which are given in Fig. 1. The first, which is denoted by g , represents the vertex interaction α between the bare state B_0 , and the two-particle basis states α ,

$$g = \sum_{\alpha} \int d^3k \left\{ |B_0\rangle G_{\alpha}^{B_0}(\mathbf{k}) \langle \alpha(\mathbf{k})| + |\alpha(\mathbf{k})\rangle G_{\alpha}^{B_0 \dagger} \langle B_0| \right\}, \quad (9)$$

where $G_{\alpha}^{B_0}$ is the momentum-dependent strength of the interaction between the bare state and each two-particle state. The momentum-dependence of these couplings is selected to reproduce the established results of chiral perturbation theory (χ PT). The second type of interaction represents the coupling between two different two-particle basis states α and β with momentum-dependent interaction strength $V_{\alpha\beta}$, and is given by

$$v = \sum_{\alpha\beta} \int d^3k \int d^3k' |\alpha(\mathbf{k})\rangle V_{\alpha\beta} \langle \beta(\mathbf{k}')|. \quad (10)$$

The interaction Hamiltonian is therefore given by

$$H_I = g + v. \quad (11)$$

B. Finite-Range Regularisation

In order to work within a finite Hilbert space, we require a renormalisation scheme. One such renormalisation scheme is FRR, which has been shown to be equivalent to other schemes, such as dimensional regularisation, while in the power-counting regime of χ PT ($m_\pi \sim m_{\text{phys}}$)[19]. It is

also equivalent to the Zeta function regularisation used in the Lüscher approach up to exponentially suppressed terms [18].

Finite-range regularisation introduces a regulator, $u(k, \Lambda)$, a function which cuts off the UV divergences at a rate governed by the regulator parameter Λ . For this study, a dipole regulator of the form

$$u(k, \Lambda) = \left(1 + \frac{k^2}{\Lambda^2}\right)^{-2}, \quad (12)$$

has been used. It has been shown that the choice of the functional form for the regulator is irrelevant in the power counting regime of χ PT [19]. The FRR expansion contains a resummation of higher-order terms that come into play as one works beyond the PCR, extending the range of utility [19–21]. The resummation ensures the FRR loop-integral contributions are smooth and approach zero for large pion masses, providing a natural explanation for the slow variation with quark mass observed in lattice QCD results. FRR provides a mechanism to exactly preserve the leading nonanalytic terms of chiral perturbation theory, including the values of the model-independent coefficients of the nonanalytic terms, even when working beyond the PCR. As one addresses larger quark masses, Λ can take on a physical role modelling the physical size of the particles. Still, studies of FRR chiral effective field theory beyond the PCR have shown the functional form of the cutoff to be unimportant [20].

As the majority of the analyses presented here are carried out at the physical point, typically regarded to be within the PCR, we commence with an expectation that the detailed functional form of the regulator is of secondary importance in our investigation.

C. Renormalisation of the Coupling

Following the approach outlined in Ref. [30], for a system with a single bare state such as that described in this paper, the full propagator $A(E)$ takes the form

$$A(E) = \frac{1}{E - m_{B_0} - \Sigma(E)}, \quad (13)$$

where $\Sigma(E)$ is the compilation of all self-energy diagrams. In particular $\Sigma(E)$ is taken such that $A(E)$ should contain a pole at the physical mass of the desired resonance. However, as we are only interested in diagrams which yield dominant contributions near the pole position, we can expand $A(E)^{-1}$ about the physical mass m . Following this, the propagator becomes

$$A(E)^{-1} = E - m_{B_0} - \Sigma(m) + (E - m) \Sigma'(m) + \Sigma^R(E), \quad (14)$$

where $\Sigma'(m)$ is the first derivative of $\Sigma(E)$ evaluated at the physical-mass expansion point m , and $\Sigma^R(E)$ contains all $(E - m)^2$ and higher-order terms in the self-energy. At the resonance position, the physical (complex) mass is given by $m = m_{B_0} + \Sigma(m)$, allowing the propagator to be rewritten

as

$$\begin{aligned} A(E)^{-1} &= E - m + (E - m) \Sigma'(m) + \Sigma^R(E), \\ &= \{1 + \Sigma'(m)\} (E - m) + \Sigma^R(E). \end{aligned} \quad (15)$$

This leads to a natural definition of the renormalised propagator

$$\tilde{A}(E) = \{1 + \Sigma'(m)\}^{-1} A(E), \quad (16)$$

where as a result, within $A(E)$ the coupling has also been renormalised by a factor of $\{1 + \Sigma'(m)\}^{-1}$. In a nonperturbative extension of EFT, this renormalisation of the coupling can become significant.

D. Infinite-Volume Scattering

In order to constrain bare state masses and potential coupling strengths, we can fit the scattering phase shifts and inelasticities calculated via the T -matrix. This can be obtained by solving the coupled-channel integral equations,

$$\begin{aligned} T_{\alpha\beta}(k, k'; E) &= \tilde{V}_{\alpha\beta}(k, k', E) \\ &+ \sum_{\gamma} \int dq q^2 \frac{\tilde{V}_{\alpha\gamma}(k, q, E) T_{\gamma\beta}(q, k'; E)}{E - \omega_{\gamma}(q) + i\epsilon}, \end{aligned} \quad (17)$$

where $\omega_{\gamma}(q) = \sqrt{q^2 + m_{\gamma M}^2} + \sqrt{q^2 + m_{\gamma B}^2}$. We have also defined the coupled-channel potential $\tilde{V}_{\alpha\beta}$ for some bare state B_0 as

$$\tilde{V}_{\alpha\beta}(k, k', E) = \frac{G_{\alpha}^{B_0 \dagger}(k) G_{\beta}^{B_0}(k')}{E - m_{B_0}} + V_{\alpha\beta}(k, k'). \quad (18)$$

The phase shifts and inelasticity however are extracted from the unitary S -matrix, which is related to the T -matrix by

$$S_{\alpha\beta}(E) = \delta_{\alpha\beta} - 2i\pi\sqrt{\rho_{\alpha}\rho_{\beta}} T_{\alpha\beta}(k_{\text{on},\alpha}, k_{\text{on},\beta}; E), \quad (19)$$

where $k_{\text{on},\alpha}$ is the on-shell momentum in channel α , and ρ_{α} is defined as

$$\rho_{\alpha} = \frac{\sqrt{k_{\text{on},\alpha}^2 + m_{\alpha M}^2} \sqrt{k_{\text{on},\alpha}^2 + m_{\alpha B}^2}}{E} k_{\text{on},\alpha}. \quad (20)$$

The inelasticity, η_{α} , and phase shift, δ_{α} , are then calculated from

$$S_{\alpha\alpha}(E) = \eta_{\alpha} \exp(2i\delta_{\alpha}). \quad (21)$$

Using this formalism, the position of any poles in the S -matrix can be found by solving for the complex energy E which satisfies $T(k, k'; E)^{-1} = 0$.

E. Finite-Volume Matrix Method

On a three-dimensional, cubic lattice of volume L^3 , the allowed momentum is discretised to

$$\mathbf{k}_n = \frac{2\pi}{L} \mathbf{n}, \quad \mathbf{n} = (n_x, n_y, n_z), \quad (22)$$

where n_x, n_y , and n_z can take any integer values. As a result of this, the integrals over momentum in Eq. (8) to Eq. (10) undergo discretisation of the form

$$\int d^3k \rightarrow \sum_{\mathbf{n} \in \mathbb{Z}^3} \left(\frac{2\pi}{L} \right)^3. \quad (23)$$

For P -wave scattering however, at a sufficiently large L we can approximate spherical symmetry and consider only the degenerate momentum states. For a discussion on the effects of this approximation and partial wave mixing, see Ref. [31]. These degenerate momentum states are labelled k_n , where we have defined the integer $n = n_x^2 + n_y^2 + n_z^2$. We can represent the degeneracy of each k_n by defining a function $C_3(n)$, which counts the number of ways the squared integers n_x^2, n_y^2 , and n_z^2 can sum to each n . Some example values of this function are $C_3(2) = 12$, and $C_3(7) = 0$, as there are no combinations of square integers that sum to 7. Using this definition, the three-dimensional finite sums undergo the transformation

$$\sum_{\mathbf{n} \in \mathbb{Z}^3} \rightarrow \sum_{n \in \mathbb{Z}} C_3(n). \quad (24)$$

As our regulator parameter Λ creates a momentum cutoff, this allows the Hamiltonian matrix to have a finite size. In order to find the extent of the momentum cutoff (k_{\max}) generated by Λ , for a smooth regulator $u(k, \Lambda)$ such as the dipole regulator defined in Eq. (12), we must choose some minimum value of the regulator size, u_{\min} . This value should be chosen such that it both minimises the size of the matrix to reduce computational requirements, and allows sufficient contributions from all significant basis states. A value of $u_{\min} = 0.01$ was chosen to balance these two requirements. Inserting u_{\min} into equation Eq. (12) and solving for the resulting k_{\max} gives a maximum momentum of

$$k_{\max} = \Lambda \sqrt{u_{\min}^{-\frac{1}{2}} - 1}. \quad (25)$$

This can then be used to solve for the size of the Hamiltonian matrix from Eq. (22),

$$n_{\max} = \left(\frac{k_{\max} L}{2\pi} \right)^2. \quad (26)$$

Due to the discretisation process, the potentials in Eq. (9) and Eq. (10) undergo a scaling due to finite-volume factors. These finite-volume potentials are labelled as $\bar{G}_\alpha^{B_0}(k)$ and $\bar{V}_{\alpha\beta}(k, k')$, and the relationship between the finite and infinite volume potentials will be outlined in the next section.

F. Finite-Volume Factors

In order to calculate the scaling factors due to the finite volume, we consider the relationship between poles in the S -matrix, and solutions to the eigenvalue equation of the Hamiltonian. Considering a simple toy system, with a single bare state, and a single two-particle scattering state which only couples to the bare state with strength $G(k)$. This scenario is one typically considered in leading one-loop χ PT calculations. Using the notation defined in Sec. III E, in finite-volume this interaction strength can be written as $\bar{G}(k)$. The Hamiltonian for such a system therefore takes the form

$$H = \begin{pmatrix} m_{B_0} & \bar{G}(k_1) & \bar{G}(k_2) & \dots \\ \bar{G}(k_1) & \omega_\alpha(k_1) & 0 & \dots \\ \bar{G}(k_2) & 0 & \omega_\alpha(k_2) & \ddots \\ \vdots & \vdots & \ddots & \ddots \end{pmatrix}. \quad (27)$$

Due to the sparse nature of this matrix, an exact expression can be written for solutions of the eigenvalue equation $|H - E \mathbb{I}| = 0$, giving

$$E = m_{B_0} - \sum_n \frac{\bar{G}^2(k_n)}{\omega(k_n) - E}. \quad (28)$$

It is worth noting that upon replacing E on the RHS with the renormalised mass m_B , one can make contact with finite-volume χ PT, thus defining the relationship between $G(k)$ and $\bar{G}(k)$.

To define this relationship, we return to infinite-volume. For the simple system defined in this section, the absence of any interactions between different two-particle states means that Eq. (18) reduces to

$$\tilde{V}(k, k'; E) = \frac{G(k) G(k')}{E - m_{B_0}}. \quad (29)$$

For a separable potential such as this, the associated T -matrix is also separable, and is able to be written as

$$T(k, k'; E) = G(k) t(E) G(k'), \quad (30)$$

Substituting this into Eq. (17) therefore gives an expression for $t(E)$ in the form

$$t(E) = \left[m_{B_0} - E - \int_0^\infty dq q^2 \frac{G^2(q)}{E - \omega(q) + i\epsilon} \right]^{-1}. \quad (31)$$

As the S -matrix is proportional to $t(E)$, poles in the S -matrix can be found by solving for $t^{-1}(E) = 0$, giving

$$E = m_{B_0} - \int_0^\infty dq q^2 \frac{G^2(q)}{E - \omega(q) + i\epsilon}. \quad (32)$$

Using the fact that for a spherically symmetric momentum space,

$$\int dq q^2 = \int dq q^2 \int \frac{d\Omega}{4\pi} = \int \frac{d^3q}{4\pi}, \quad (33)$$

we can make use of Eq. (23) and Eq. (24) to obtain an expression for the finite-volume energies in terms of the infinite-volume potentials,

$$E = m_{B_0} - \sum_n \frac{C_3(n)}{4\pi} \left(\frac{2\pi}{L}\right)^3 \frac{G^2(k_n)}{\omega(k_n) - E}. \quad (34)$$

By comparing this expression to Eq. (28), it can be seen that the finite and infinite-volume potentials are related according to

$$\bar{G}^2(k_n) = \frac{C_3(n)}{4\pi} \left(\frac{2\pi}{L}\right)^3 G^2(k_n). \quad (35)$$

Having found this relation, we can therefore return to the general notation for interaction strengths defined in Sec. III A, giving the finite-volume potentials

$$\bar{G}_\alpha^{B_0}(k_n) = \sqrt{\frac{C_3(n)}{4\pi}} \left(\frac{2\pi}{L}\right)^{\frac{3}{2}} G_\alpha^{B_0}(k_n), \quad (36)$$

$$\bar{V}_{\alpha\beta}(k_n, k_m) = \sqrt{\frac{C_3(n)}{4\pi}} \sqrt{\frac{C_3(m)}{4\pi}} \left(\frac{2\pi}{L}\right)^3 V_\beta^\alpha(k_n, k_m). \quad (37)$$

IV. SINGLE CHANNEL ANALYSIS

A. Fitting Experimental Data

In order to generate a finite-volume energy spectrum, we can obtain values for the bare mass and potential coupling strengths by fitting experimental phase shifts. In the simplest case, we can consider the πN system to be described by a single bare state, and with only the πN scattering channel contributing. In this case, we fit to experimental data below the $\pi\Delta$ threshold at approximately 1350 MeV. For the interaction between the bare Δ and the πN scattering state, the coupling from Eq. (9) is taken from Ref. [17], and has the form

$$G_{\pi N}^\Delta(k) = \frac{g_{\pi N}^\Delta}{m_\pi^{\text{phys}}} \frac{k}{\sqrt{\omega_\pi(k)}} u(k, \Lambda), \quad (38)$$

where $\omega_\pi(k) = \sqrt{k^2 + m_\pi^2}$, $u(k, \Lambda)$ is the regulator defined in Eq. (12), and the inclusion of m_π^{phys} allows the coupling $g_{\pi N}^\Delta$ to be dimensionless.

For the πN - πN interaction of Eq. (10), the separable potential from Ref. [32] is used, which takes the form

$$V_{\pi N, \pi N}(k, k') = \frac{v_{\pi N, \pi N}}{(m_\pi^{\text{phys}})^2} \frac{k}{\omega_\pi(k)} \frac{k'}{\omega_\pi(k')} u(k, \Lambda) u(k', \Lambda). \quad (39)$$

While in principle the regulator parameter in $G_{\pi N}^\Delta(k)$ and in $V_{\pi N, \pi N}(k, k')$ can take different values, in this study they will be fixed to the same value to simplify the analysis.

Inserting these into the relativised Lippmann-Schwinger equation from Eq. (17), we can extract the πN phase shift $\delta_{\pi N}$. Using these phase shifts, and choosing $\Lambda = 0.8$ GeV

TABLE I. Single-channel fit parameters constrained to πN scattering data [34]. Fits I and II contain a single-particle basis state $|\Delta_0\rangle$, while Fit III does not.

Parameter	With $ \Delta_0\rangle$		No $ \Delta_0\rangle$
	Fit I	Fit II	Fit III
$m_{\Delta}^{(0)}/\text{GeV}$	1.3589	1.3720	-
$g_{\pi N}^\Delta$	0.1762	0.0006	-
$v_{\pi N, \pi N}$	-0.0286	-0.0029	-0.0029
Λ/GeV	0.8000	8.0000	8.0000
α_0/GeV^{-1}	0.6489	-	-
Pole / GeV	$1.211 - 0.049i$	$1.207 - 0.044i$	$1.205 - 0.045i$

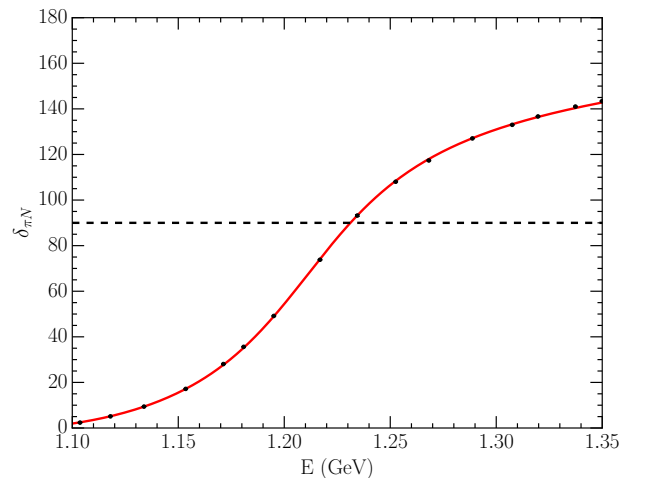


FIG. 2. P -wave πN phase shifts for a system with a bare state, where the solid points are experimental data obtained from Ref. [34], the solid line is the fit using HEFT to the data, and the dashed line represents a phase shift of 90 degrees. The parameter set producing this curve is given by Fit I of Table I.

for now, we can fit πN scattering data, such as that from Ref. [33]. The parameter set for this fit can be seen in Table I where a bare state is included, and the phase shifts corresponding to this fit are illustrated in Fig. 2. As can be seen in Table I, using the 0.8 GeV fit (Fit I) we calculate a pole position of approximately $1.211 - 0.049i$ GeV. This is comparable to the pole position of the Δ as quoted by the Particle Data Group (PDG)[35], which takes the value of approximately $1.210 - 0.050i$ GeV.

B. Finite-Volume Dependence

Using the parameters found by fitting the scattering data, the matrix Hamiltonian can be constructed. For the single-channel system, the free Hamiltonian from Eq. (8) can be writ-

ten as

$$H_0 = \text{diag} \left(m_\Delta^{(0)}, \omega_{\pi N}(k_1), \omega_{\pi N}(k_2), \dots \right), \quad (40)$$

where $\omega_{\pi N}(k_i) = \sqrt{k^2 + m_\pi^2} + \sqrt{k^2 + m_N^2}$. The interaction Hamiltonian from Eq. (11) can be written in matrix form as

$$H_I = \begin{pmatrix} 0 & \bar{G}_{\pi N}^\Delta(k_1) & \bar{G}_{\pi N}^\Delta(k_2) & \dots \\ \bar{G}_{\pi N}^\Delta(k_1) & \bar{V}_{\pi N, \pi N}(k_1, k_1) & \bar{V}_{\pi N, \pi N}(k_1, k_2) & \dots \\ \bar{G}_{\pi N}^\Delta(k_2) & \bar{V}_{\pi N, \pi N}(k_2, k_1) & \bar{V}_{\pi N, \pi N}(k_2, k_2) & \dots \\ \vdots & \vdots & \ddots & \vdots \end{pmatrix}, \quad (41)$$

and so the full Hamiltonian can be constructed as $H = H_0 + H_I$. In the simplest possible case where $v_{\pi N, \pi N} = 0$, and therefore the only interaction present is the $\Delta_0 \rightarrow \pi N$ vertex, the eigenvalues of the matrix Hamiltonian can be solved exactly[17]. Solving the eigenvalue equation $|H - E\mathbb{I}| = 0$, the eigenvalues are found as solutions of

$$E = m_\Delta^{(0)} - \sum_{n=1}^{n_{\max}} \frac{\bar{G}_{\pi N}^\Delta(k_n)^2}{\omega_{\pi N}(k_n) - E}. \quad (42)$$

We note that by taking the limit for this equation where $L, n_{\max} \rightarrow \infty$, and associating the energy E on the right-hand side with the renormalised Δ mass m_Δ , this expression for the eigenvalues is restored to the one-loop correction to the Δ mass,

$$m_\Delta = m_\Delta^{(0)} - \left(\frac{g_{\pi N}^\Delta}{m_\pi^{\text{phys}}} \right)^2 \int_0^\infty \frac{k'^4 u(k', \Lambda)^2 dk'}{\omega_\pi(k') [m_\Delta - \omega_{\pi N}(k') + i\epsilon]}. \quad (43)$$

We use a numerical routine to solve for the eigenmodes of H . Varying the lattice volume L , we can generate the finite-volume energy spectrum for this system, as seen in Fig. 3. In order to observe the contributions from the single-particle basis state, $|\Delta_0\rangle$, to the energy eigenvalues, it is convenient to highlight the states which have the largest contribution from $|\Delta_0\rangle$. This can be seen in Fig. 4, where the three different highlighting methods show the states with the first, second and third highest probabilities for the single-particle $|\Delta_0\rangle$ basis-state contribution.

In Sec. IV D, these states will be identified as eigenstates having the largest overlap with lattice QCD eigenstates excited by three-quark interpolating fields, and therefore can be considered the states which are first, second and third most likely to be observed in a lattice QCD calculation with three-quark operators.

C. Regulator Parameter Dependence

In the power-counting regime of χ EFT, which includes the region $m_\pi \sim m_\pi^{\text{phys}}$, there is no dependence of any results on the regulator parameter Λ . We therefore expect that the eigenvalues of the Hamiltonian in HEFT will be Λ independent to a very good approximation and to test this we fit the scattering

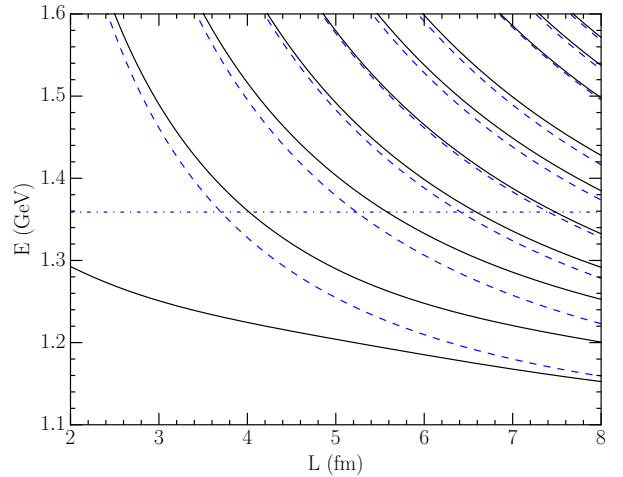


FIG. 3. Lattice volume dependence of the energy eigenvalues of the Hamiltonian. The solid lines represent the energy eigenvalues following from Fit I of Table I. The horizontal dot-dashed line is the bare mass and the curved dashed lines are the non-interacting πN basis states at $k = 2\pi/L, 2\sqrt{2}\pi/L, \dots$

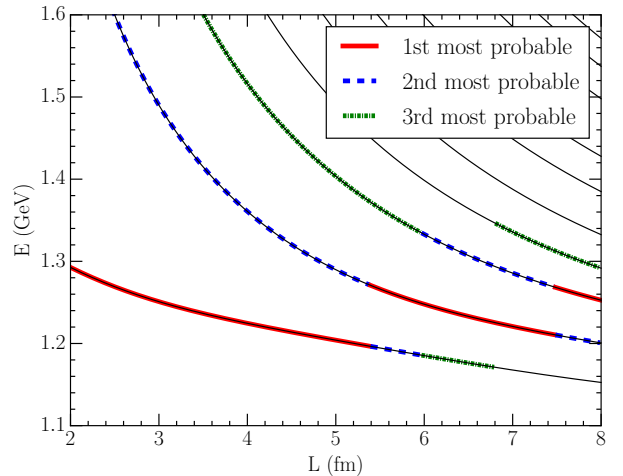


FIG. 4. Lattice volume dependence of the energy eigenvalues of the Hamiltonian from Fit I of Table I. The solid (red), dashed (blue) and dot-dashed (green) highlights on the eigenvalues correspond to the states with the largest, second-largest and third-largest contribution from the bare basis state $|\Delta_0\rangle$ respectively.

data for values of Λ varying from 0.6 GeV to 8 GeV. The upper limit selected here is interesting as one can describe the experimental data reasonably well without a single-particle basis state as illustrated in Fig. 5.

Using each fit to the experimental data for $E \lesssim 1350$ MeV, we can then solve for the eigenvalues of the finite-volume Hamiltonian and plot the lowest lying states to check for any Λ -dependence of these states.

Indeed, as we see in Fig. 6, the lowest lying states on both lattice volumes are completely Λ -independent provided that these eigenstates lie below the $\pi\Delta$ threshold, which is where the theory is constrained to fit the phase shift data.

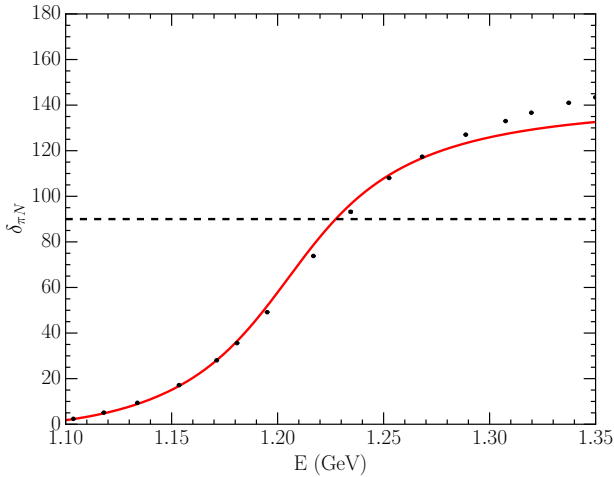


FIG. 5. P -wave πN phase shifts for a system with no single-particle state, where the solid points are experimental data obtained from Ref. [34], the solid line is the fit using HEFT to the data, and the dashed line represents a phase shift of 90 degrees. The parameter set producing this curve is given by Fit III of Table I.

While there is no observable Λ -dependence for the eigenvalues in the energy region where the HEFT has been constrained by data, we are also interested in how the regulator parameter could affect the physical interpretation of the lattice QCD results.

In particular, it is of interest to see how the location of the state dominated by the single-particle basis state, $|\Delta_0\rangle$, is affected by Λ . This can be investigated by illustrating the values of the eigenvectors from the Hamiltonian matrix. As the eigenvectors represent the contribution of each basis state to the final eigenstate, we can plot these as a function of Λ to observe how the $|\Delta_0\rangle$ contribution to each eigenstate depends on the regulator parameter.

In Fig. 7 and Fig. 8, we show the Λ -dependence of the two lowest lying eigenstates for two different lattice volumes. It is clear that unlike the eigenvalues, the eigenvectors have a strong Λ -dependence and, in fact, the position of the state which is dominated by the bare Δ is not always Λ -independent. This is particularly clear at smaller lattice volumes, where the bare contribution to the ground state decreases as Λ . For the larger volume at $L = 5.0$ fm, the first excited state varies between being associated with the the single-particle contribution and the bare state contribution, and is more stable to Λ variation.

Probing the Λ dependence of these eigenvectors also shows how, as Λ increases, the contribution from the bare Δ becomes distributed throughout the higher eigenstates, rather than being concentrated in the ground state. As can be seen in Table I, the strength of the coupling $g_{\pi N}^\Delta$ required to describe the scattering data at large values of Λ significantly decreases, and indeed it seems as though a bare Δ may not be required at all. In fact, with a very large regulator parameter, the scattering data can be fit just as well with and without a bare state [36, 37]. It was found that $\Lambda = 8.0$ GeV is the smallest value of Λ which gives a good description of the data. This fit is labelled Fit

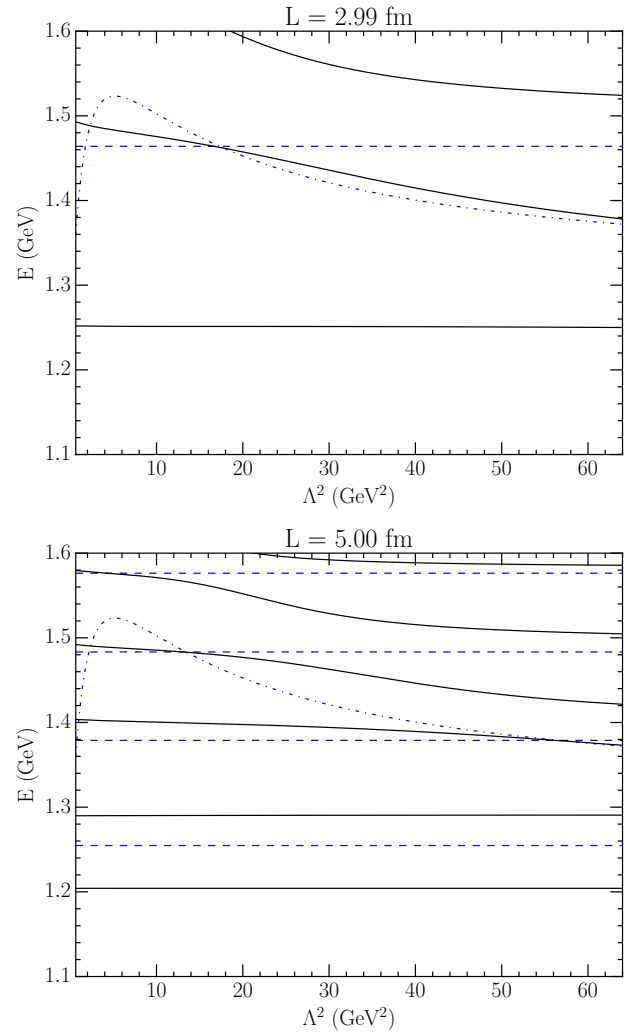


FIG. 6. Dependence of the lowest lying eigenvalues of the finite-volume Hamiltonian on the regulator parameter Λ for two different lattice sizes, where Λ is varying from 0.6 to 8.0 GeV. The solid (black) lines are the eigenvalues, the horizontal dashed (blue) lines are πN basis states, and the curved dot-dashed (blue) line is the mass of the bare Δ . The Hamiltonian was constrained to experimental data with $E \lesssim 1350$ MeV.

III in Table I, and is illustrated in Fig. 5. Here we only have $v_{\pi N \pi N}$ as a free parameter, the value of which can be found in Table I.

Comparing Fig. 2 and Fig. 5, both fits give a good description of the data near the resonance position, though the inclusion of a single-particle basis state improves the description of the data at higher energies.

While these two scenarios can reproduce scattering data at the physical pion mass, an important strength of HEFT lies in its capacity to compare with and interpret lattice QCD results in the region beyond the physical pion mass. By observing the pion mass dependence of these states in lattice QCD versus the predictions of HEFT for different choices of interactions, one can obtain some insight into which system of interactions, and hence which physical picture, best describes the Δ .

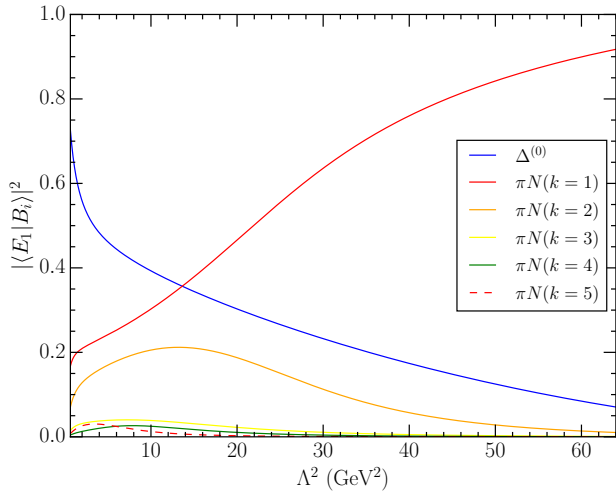


FIG. 7. Dependence of the energy-eigenstate basis-state structure on the regulator parameter Λ , where Λ is varying from 0.6 to 8.0 GeV, for a lattice size of $L = 2.99$ fm. Only the ground state is shown, as all higher eigenstates lie above the fitting threshold of $E = 1350$ MeV and thus are not physically constrained.

D. Comparison with lattice QCD

To generalise these finite-volume energies to larger-than-physical pion masses, we take the pion mass dependence of the bare state to vary linearly in m_π^2 , taking the form

$$m_\Delta^{(0)} = m_\Delta^{(0)}\Big|_{\text{phys}} + \alpha_0 \left(m_\pi^2 - m_\pi^2\Big|_{\text{phys}} \right), \quad (44)$$

as one expects in any quark model.

The value for the mass slope α_0 is found by performing a single-parameter fit to lattice QCD results for the ground state Δ at a lattice size of $L = 2.99$ fm, as given by the PACS-CS collaboration [14]. At this volume the ground state is dominated by the three-quark-like bare state, as can be seen in Fig. 4.

In considering pion masses away from the chiral limit, we adopt the approach of χ PT where couplings are fixed and variation with pion mass is contained within the higher-order terms of the expansion [38]. Chiral limit couplings are approximated by our analysis of scattering data necessarily at the physical point.

We begin by considering $\Lambda = 0.8$ GeV and constraining α_0 by a fit to the lattice QCD results. The fit value is reported in Table I and the fit is illustrated in the upper-left panel of Fig. 9. In principle this process can be repeated for other values of Λ . However, with the simple residual series of Eq. (44), only the $\Lambda = 0.8$ GeV fit approaches the lattice QCD results. While different values of α_0 for each fit were considered, varying α_0 was found to be unhelpful in attempting to reproduce the lattice energies at larger pion masses. For the purpose of illustration in Fig. 9, the value for α_0 from the $\Lambda = 0.8$ GeV fit has been applied to all other values of Λ considered. We note the $\Lambda = 8.0$ GeV case no longer requires a bare state to describe the experimental scattering data. As a result, there is

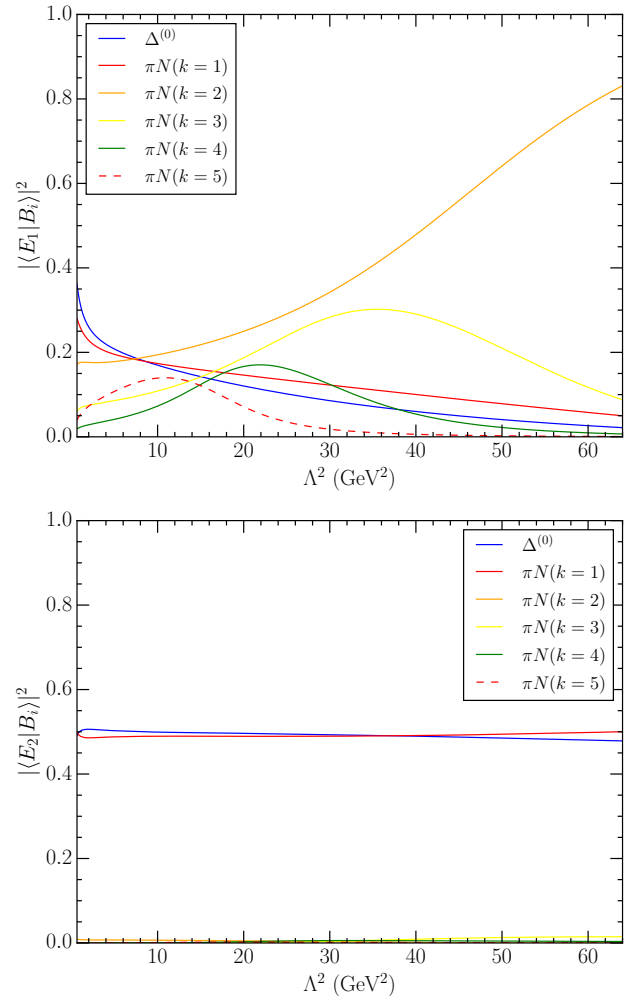


FIG. 8. Dependence of the energy-eigenstate basis-state structure on the regulator parameter Λ , where Λ is varying from 0.6 to 8.0 GeV, for a lattice size of $L = 5$ fm. The two lowest-lying energy eigenstates of the finite-volume Hamiltonian are investigated. The upper plot shows the eigenvectors for the ground state, while the lower plot shows the first excited state.

no opportunity for residual-series contributions.

While the scattering data can be described with any of these values of Λ , and both with and without a bare state, there are significant differences in the pion-mass dependence of the spectra. Of the regulator parameters considered, only $\Lambda = 0.8$ GeV is able to describe the lattice energies away from the physical pion mass.

However, it is important to understand that this result follows directly from the simple ansatz considered for the pion mass dependence of the bare-baryon basis state in Eq. (44). If one allows the residual series expansion to contain higher orders of m_π^2 , then one could certainly run a curve through the lattice results.

This is precisely the situation revealed when comparing FRR EFT descriptions of lattice QCD results with the dimensional-regularisation approach. For example, Fig. 9 of Ref. [39] illustrates a dimensional-regularisation style expansion

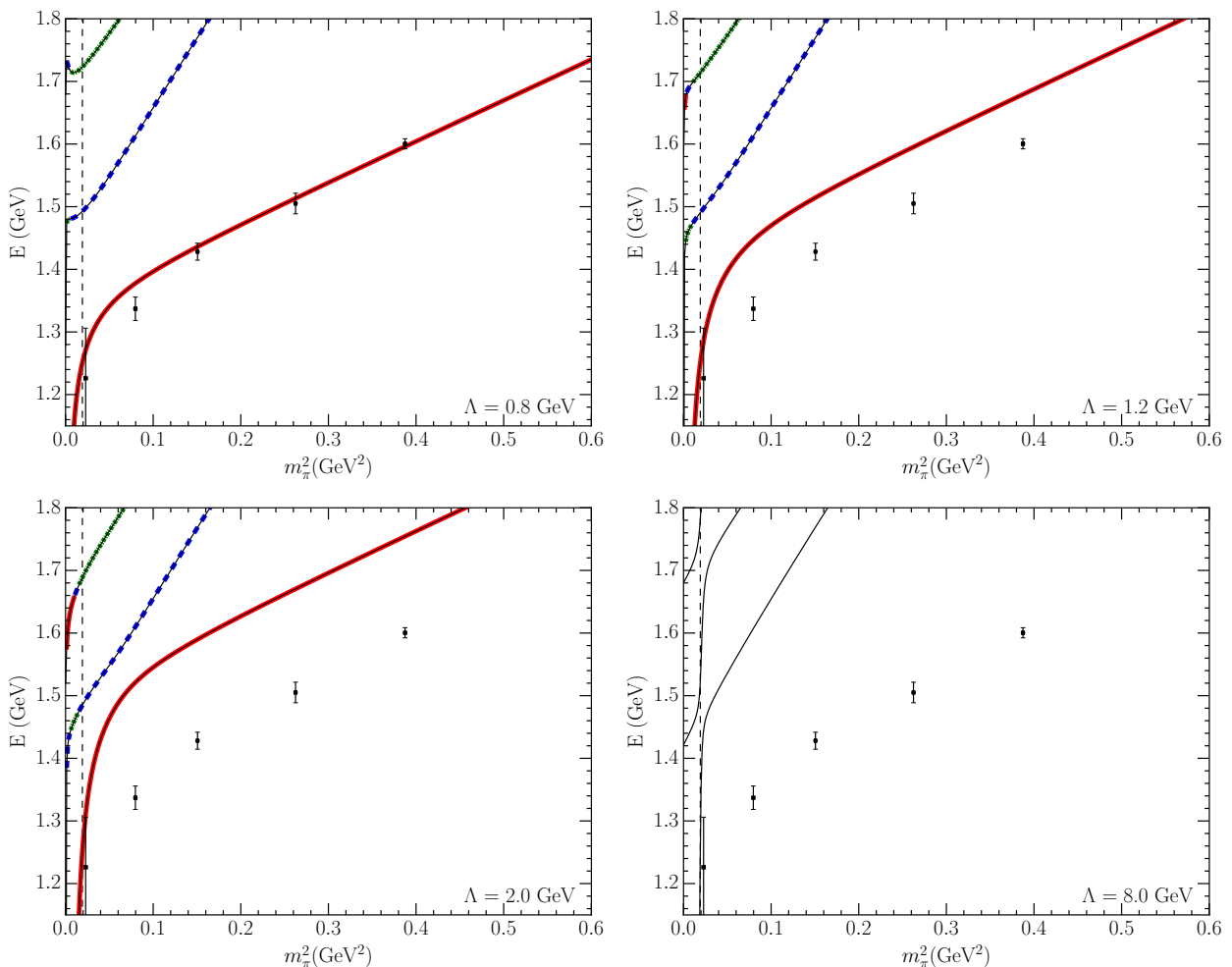


FIG. 9. Pion mass dependence of the finite-volume HEFT eigenvalues at $L = 2.99$ fm for increasing values of the regulator parameter Λ , where no bare basis state is present for $\Lambda = 8.0$ GeV. The solid black curves illustrate the finite-volume energy levels predicted by HEFT from fits to experimental phase shifts. These lines are dressed by solid (red), dashed (blue) and dot-dashed (green) highlights indicating states with the largest, second-largest and third-largest contribution from the bare basis state $|\Delta_0\rangle$ respectively. Lattice QCD results for lowest-lying Δ masses, denoted by the (black) points, are from the PACS-CS collaboration [14]. As these lattice results follow from local three-quark operators, they are expected to lie on a solid (red) energy eigenstate. The vertical dashed (black) line illustrates the physical pion mass.

sion of an FRR EFT description of lattice QCD results. There, 14 terms in the residual series expansion up to and including m_π^{26} are required to reach $m_\pi^2 = 0.2$ GeV², and 26 terms up to and including m_π^{50} are required to reach $m_\pi^2 = 0.3$ GeV². The lesson learned is that if hard momenta are allowed to flow through effective field propagators, large errors are made. The contributions of the residual series terms will necessarily be large to correct for these short-distance errors. Thus while it is possible to make the curves go through the lattice QCD results in Fig. 9 via a more complicated pion-mass dependence for the residual-series coefficients of the bare-baryon basis state there is little merit in doing so. The physics associated with the interactions of the Hamiltonian and its associated eigenvectors contain large errors that are corrected by the quark-mass dependence of the bare baryon basis state. In this case the eigenvectors of the Hamiltonian will reflect the erroneous incorporation of short-distance physics.

Finally, we note that without a bare state, there is no avenue for bringing the HEFT predictions into agreement with the lattice QCD results.

In summary, to keep the terms of the residual series expansion small, such that the physics resides within the interactions of the Hamiltonian, one needs a phenomenologically motivated regulator to capture the bulk of the physics correctly. This conclusion is in accord with findings reached within the cloudy bag model [29, 37].

V. TWO CHANNEL ANALYSIS

A. Fitting Experimental Data

The power of the constraints provided by experimental scattering data on the predictions of HEFT is manifest in Fig. 7

TABLE II. Two-channel fit parameters constrained to πN scattering data up to 1650 MeV. Here, Λ is fixed for each of the two fits while all other parameters are allowed to vary.

Parameter	Fit IV	Fit V
$m_{\Delta}^{(0)}/\text{GeV}$	1.3837	1.4405
$g_{\pi N}^{\Delta}$	0.1286	0.1041
$g_{\pi\Delta}^{\Delta}$	0.1324	0.0171
$v_{\pi N, \pi N}$	-0.0103	-0.0233
$v_{\pi N, \pi\Delta}$	-0.0811	-0.0220
$v_{\pi\Delta, \pi\Delta}$	-0.0015	-0.0645
Λ/GeV	0.8000	1.2000
α_0/GeV^{-1}	0.5819	-
Pole 1 / GeV	$1.210 - 0.049i$	$1.211 - 0.049i$
Pole 2 / GeV	$1.434 - 0.207i$	$1.449 - 0.053i$

and Fig. 8. Thus, it is desirable to extend the energy range considered beyond the $\pi\Delta$ threshold in an effort to describe excitations of the Δ , in addition to the lowest lying resonance. To proceed, we will conduct a similar analysis including higher energies by introducing a second scattering channel, a $\pi\Delta$ channel.

Previously we were able to describe the scattering data to 1350 MeV with a πN scattering channel. To describe the data up to 1650 MeV, we require the next $\pi\Delta$ scattering channel to account for inelasticity beyond the $\pi\Delta$ threshold. To describe the interactions in the $\pi\Delta$ channel, we use the same functional form as Eq. (38) to describe the $\Delta^{(0)} \rightarrow \pi\Delta$ interaction, and the same potential as Eq. (39) to describe the $\pi\Delta \rightarrow \pi\Delta$ and $\pi\Delta \rightarrow \pi N$ interactions. This introduces three new fit parameters for the system: $g_{\pi\Delta}^{\Delta}$, $v_{\pi N\pi\Delta}$, and $v_{\pi\Delta\pi\Delta}$.

In fitting the experimental data, we must reproduce both the πN phase shift $\delta_{\pi N}$, and the inelasticity η . Unlike the single-channel case, the increased number of parameters and the inclusion of the inelasticity make it difficult to fit the data for larger values of Λ . Variation in the parameters is more unstable, and good fits to the scattering data above approximately $\Lambda = 1.2$ GeV are elusive.

For the SAID data up to 1650 MeV, we are able to obtain fits between $\Lambda = 0.8$ GeV and $\Lambda = 1.2$ GeV. The fit parameters at these two limits for Λ are presented in Table II. While both fits generate a pole at approximately the PDG pole position of $1.210 - 0.050i$ GeV, they are not able to describe the scattering data equally well. It is also worth noting that a second pole was found for each of the two sets of fit parameters, though with significantly different values for the imaginary components of each pole. These values are somewhat comparable to the PDG pole position for the $\Delta(1600)$ at approximately $(1.510 \pm 0.050) - (0.135 \pm 0.035)i$ GeV [35], though the imaginary component of the second pole for Fit V is considerably smaller.

As illustrated in Fig. 10, both fits are able to describe the

scattering phase shifts up to 1650 MeV; however, only the smaller value of $\Lambda = 0.8$ GeV is able to give a good description of the inelasticity.

In order to observe the effect these differing fits have on the corresponding lattice energy levels, we explore the lattice volume and Λ dependence of the finite-volume eigenmodes in the next two sections.

B. Finite-Volume Dependence

Adding an additional channel to the Hamiltonian matrix only requires an additional row/column for each channel at each momentum k_n . Therefore the free Hamiltonian takes the form

$$H_0 = \text{diag} \left(m_{\Delta}^{(0)}, \omega_{\pi N}(k_1), \omega_{\pi\Delta}(k_1), \omega_{\pi N}(k_2), \omega_{\pi\Delta}(k_2), \dots \right). \quad (45)$$

Similarly, we can write the interaction Hamiltonian as

$$H_I = \begin{pmatrix} 0 & \bar{G}_{\pi N}^{\Delta}(k_1) & \bar{G}_{\pi\Delta}^{\Delta}(k_1) & \dots \\ \bar{G}_{\pi N}^{\Delta}(k_1) & \bar{V}_{\pi N, \pi N}(k_1, k_1) & \bar{V}_{\pi N, \pi\Delta}(k_1, k_1) & \dots \\ \bar{G}_{\pi\Delta}^{\Delta}(k_1) & \bar{V}_{\pi\Delta, \pi N}(k_1, k_1) & \bar{V}_{\pi\Delta, \pi\Delta}(k_1, k_1) & \dots \\ \vdots & \vdots & \ddots & \vdots \end{pmatrix}. \quad (46)$$

Taking the Hamiltonian and solving the eigenvalue equation for varying lattice lengths, L , we can generate the finite-volume spectra seen in Fig. 11 and Fig. 12 for $\Lambda = 0.8$ GeV.

Below the $\pi\Delta$ threshold of approximately 1350 MeV, the two-channel finite-volume spectrum has the same form as the single-channel spectrum, which is to be expected as both the single-channel fit and the two-channel fit perform equally well below the $\pi\Delta$ threshold. Above this threshold, however, mixing between πN and $\pi\Delta$ basis states results in avoided level crossings. These are apparent in the energy eigenvalues above the $\pi\Delta$ threshold of 1350 MeV. For the smaller volumes where the states are forced to interact in the finite volume, the energy gaps are significant, and can be used to infer scattering observables from the finite-volume spectrum.

C. Regulator Parameter Dependence

As in the single-channel analysis reported in Sec. IV C, we proceed to understand how this finite-volume spectrum depends on the choice of the regulator parameter Λ , albeit over a smaller range of Λ . The range of Λ considered isn't a problem however, as using our single-channel results to guide us, we expect that optimal results will be obtained in the physically-motivated region around $\Lambda = 0.8$ GeV. a

The results obtained by solving for the eigenvalues of the Hamiltonian with Λ varying from 0.8 GeV to 1.2 GeV are presented in Fig. 13. Here, for both $L = 2.99$ fm and $L = 6.0$ fm, we see that, as in the single-channel case, we have Λ independence of the energy eigenvalues from Λ over the region

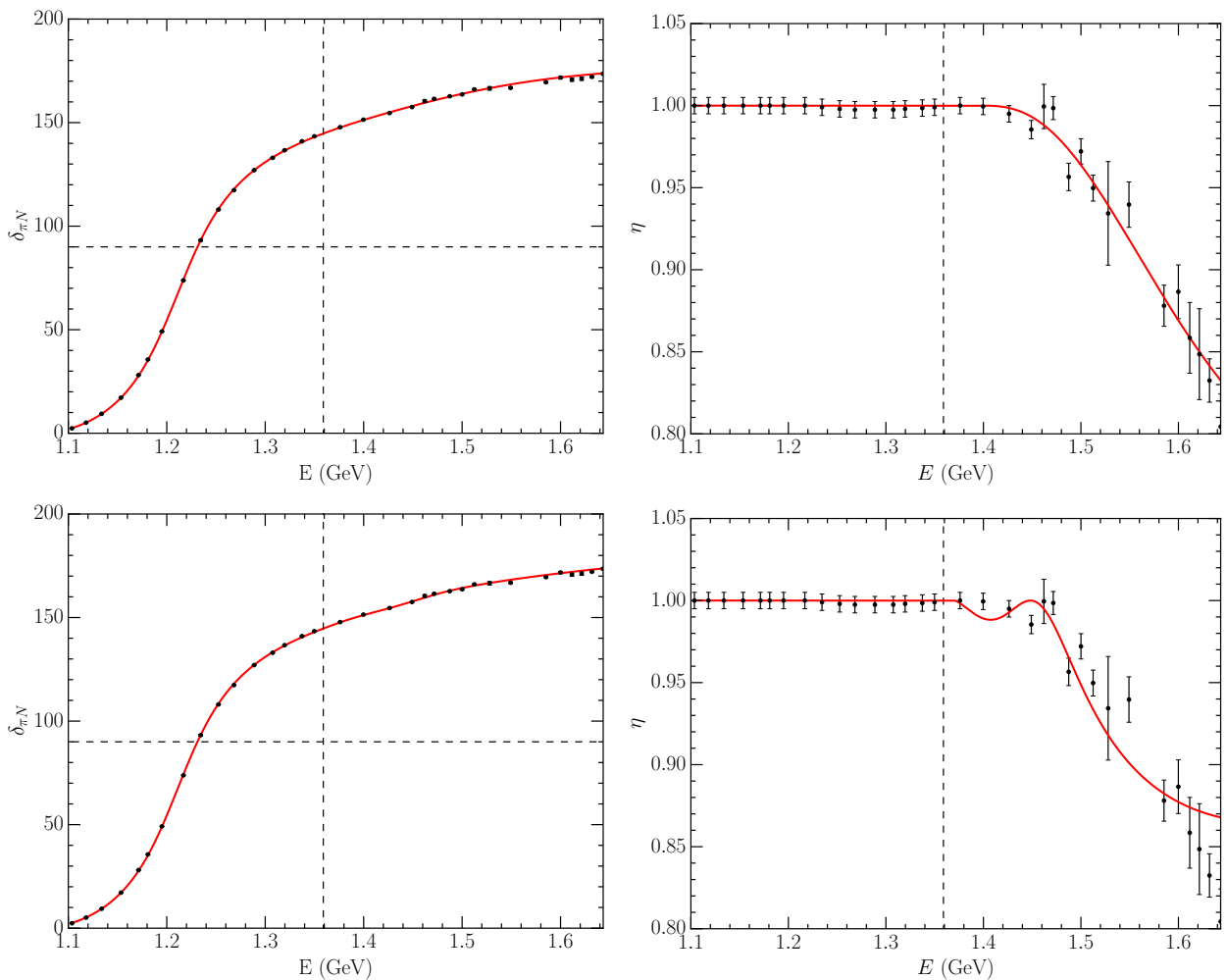


FIG. 10. P -wave πN phase shifts and inelasticities. The solid points are experimental data obtained from Ref. [34]. The solid (red) curve is the fit of HEFT to the scattering data. The horizontal dashed line highlights a phase shift of 90 degrees, while the vertical dashed line illustrates the position of the $\pi\Delta$ threshold. The upper plots illustrate the best fit when the regulator parameter $\Lambda = 0.8$ GeV (Fit IV), while the lower plots illustrate the best fit when the regulator parameter $\Lambda = 1.2$ GeV (Fit V). Only phenomenologically motivated values associated with the induced pseudoscalar form factor of a baryon are able to give a good description of the inelasticity.

where the Hamiltonian parameters are constrained by the scattering phase shift data, this time to 1650 MeV. Indeed, even the energy levels at ~ 1.7 GeV in Fig. 13 show an independence from Λ . A minor kink is observed at ~ 0.7 GeV in the mass of the bare state, this simply corresponds with minor numerical instabilities associated with the very small values of $v_{\pi N, \pi N}$ that the fitting routine tends towards at this regulator value.

Remarkably, the inability to describe the experimental inelasticity when considering larger values of Λ does not significantly affect the energy eigenvalues of the spectrum. This raises a concern on the ability of lattice QCD calculations to resolve the inelasticities in scattering data.

As in the single-channel case, it is of interest to analyse how the eigenvectors describing the composition of the energy eigenstates vary with Λ . Although we have an additional channel, the overall behaviour of the eigenvectors is similar to that observed in the single channel case. Fig. 14 illustrates the

Λ dependence of the composition. As Λ increases, enhanced short-distance mixing between the basis states replaces contributions from the bare state.

However, given that the experimental inelasticities can only be described with $\Lambda \sim 0.8$ GeV – in accord with phenomenologically motivated values associated with the induced pseudoscalar form factor of a baryon – we turn our attention to variation of the composition over the range $0.6 \leq \Lambda \leq 1.0$ GeV. Over this range, the composition of the energy eigenstates shows very little dependence on the regulator parameter. Thus, physical insight into the meson-baryon rescattering contributions to the energy eigenstates can be extracted.

D. Pion Mass Dependence of the Finite-Volume Spectrum

In the single-channel system, we were able to discover a preferred value for Λ in describing the system only by solving

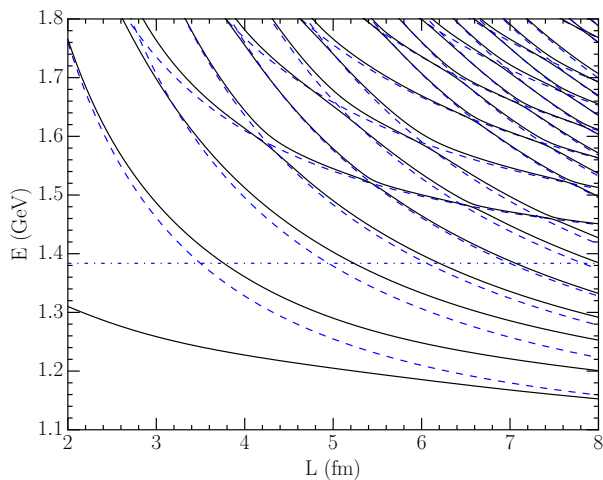


FIG. 11. Two-channel lattice volume dependence of the energy eigenvalues of the Hamiltonian for the fit to experimental data with $\Lambda = 0.8$ GeV. The solid lines represent the energy eigenvalues. The horizontal dot-dashed line is the bare mass and the curved dashed lines are the πN and $\pi\Delta$ scattering states at $k = (n_x^2 + n_y^2 + n_z^2)^{1/2} 2\pi/L$.

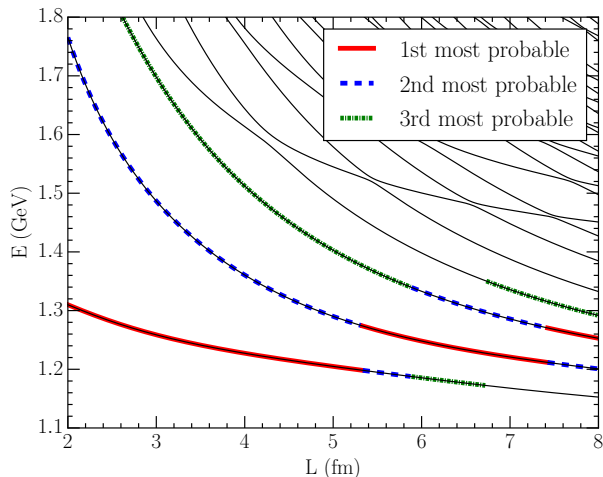


FIG. 12. Two-channel lattice volume dependence of the energy eigenvalues of the Hamiltonian for the fit to experimental data with $\Lambda = 0.8$ GeV. The solid (red), dashed (blue) and dot-dashed (green) highlights on the energy eigenvalues correspond to the states with the largest, second-largest and third-largest contribution from the bare Δ basis state respectively.

the eigenvalue equation for larger-than-physical pion masses. In the two-channel case, we have already found that increasing Λ to only 1.2 GeV results in a poor description of the experimental inelasticity. Still, it is desirable to explore how variation of the regulator parameter manifests in the pion mass dependence of the spectrum.

Results are presented in Fig. 15. As in the single-channel system, by considering a regulator parameter of $\Lambda = 0.8$ GeV, one can obtain a good description of the lattice QCD results. In contrast, consideration of a larger regulator parameter of

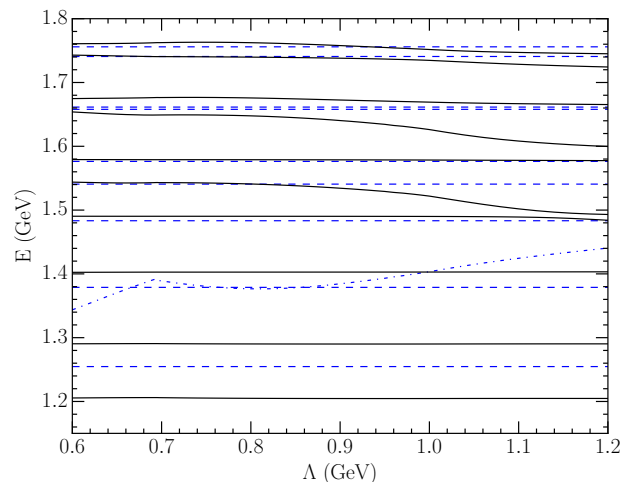
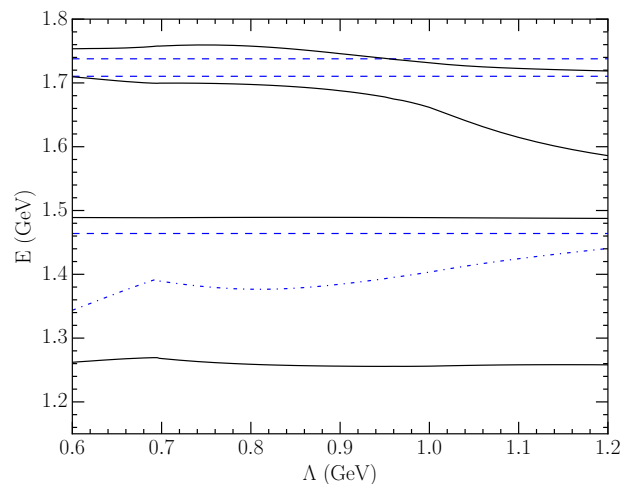


FIG. 13. Regulator parameter, Λ , dependence of the energy eigenvalues of the two scattering-channel HEFT finite-volume energy levels for the 2.99 fm lattice (top) and the 5.0 fm lattice (bottom). The solid (black) lines illustrate the energy eigenvalues, the thin horizontal dashed (blue) lines are the non-interacting energy levels of the πN and $\pi\Delta$ basis states, and the thin dash-dot (blue) curve is the mass of the bare Δ basis state.

$\Lambda = 1.2$ GeV spoils the ability to describe the lattice QCD results.

The physics underlying this result is the same as that discussed in the single channel case. The inability of the $\Lambda = 1.2$ GeV formulation to describe the lattice results is associated with the simple ansatz considered for the pion mass dependence of the bare-baryon basis state in Eq. (44). If one allows the residual series expansion to contain higher orders of m_π^2 , then one could certainly direct a curve through the lattice results.

If hard momenta are allowed to flow through effective field propagators, errors are made. The contributions of the residual series terms will necessarily be large to correct for these short-distance errors. The physics is no longer contained within the interactions of the Hamiltonian. Rather an elaborate residual series expansion is required to address the errors made in the unphysically hard interactions included in the

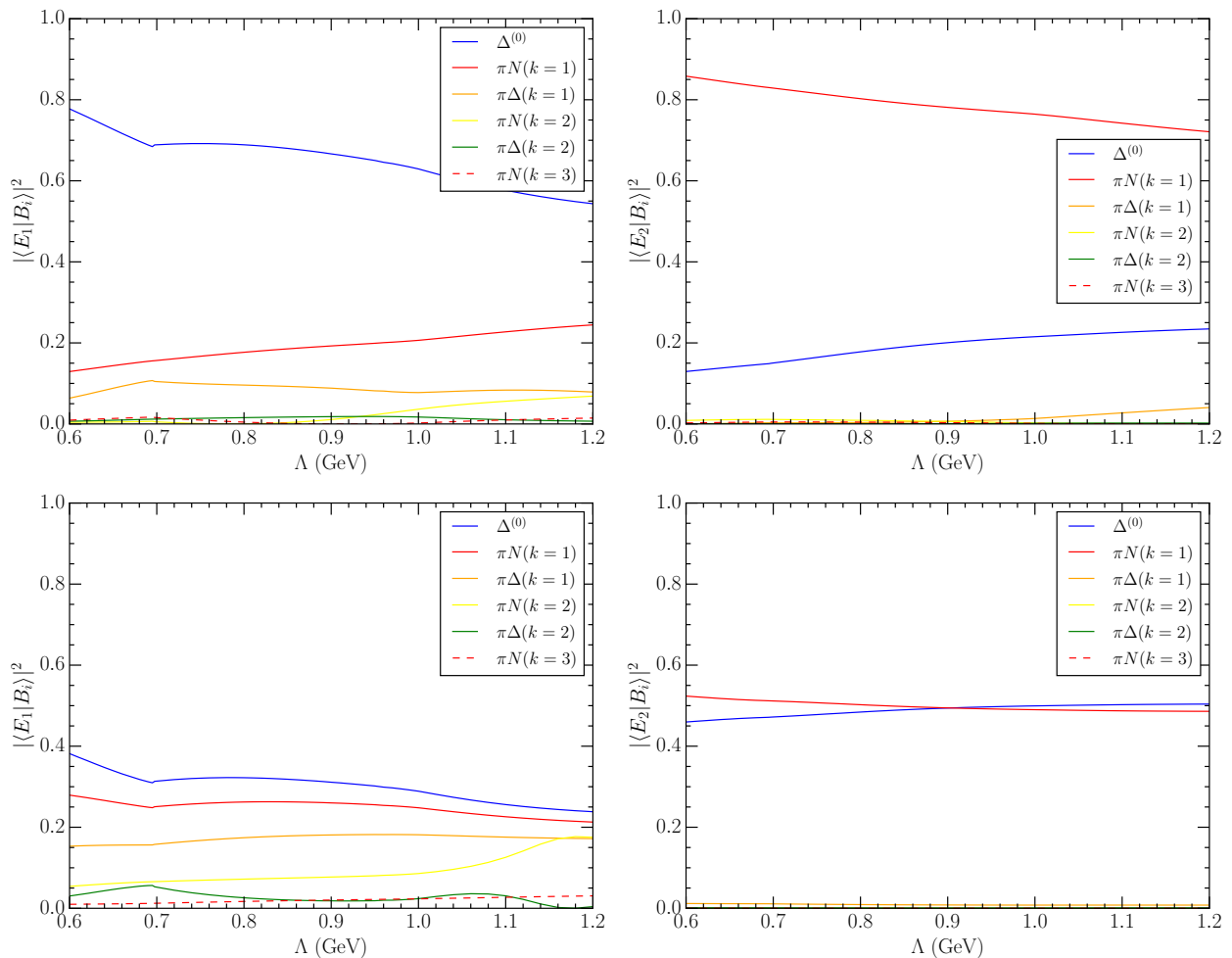


FIG. 14. Regulator parameter, Λ , dependence of the eigenvectors describing the composition of the two lowest lying energy eigenstates in the two-channel case with πN and $\pi\Delta$ scattering channels. The top two plots present results for a lattice volume of 2.99 fm, whereas the bottom two panels are for $L = 5.0$ fm. The left plot shows the eigenvectors for the lowest-lying state, while the right plot shows the next energy eigenstate. The bare basis state contributes most strongly to the lowest energy eigenstate at 2.99 fm. At 5 fm, the lowest state is only just dominated by the bare basis state, with a strong contribution from many scattering states, while the first excited eigenstate is an approximately equal mixing of the bare state and the $\pi N(k = 1)$ scattering state.

Hamiltonian with large Λ . As illustrated in Ref. [39], terms up to m_π^{26} may be required in the mass dependence of the bare baryon state to reach $m_\pi^2 = 0.2$ GeV². Moreover, the eigenvectors of the Hamiltonian formulated with large Λ will reflect the erroneous incorporation of short-distance interactions.

It is now clear that the nonperturbative extension of effective field theory in HEFT does not enjoy the same freedom in selecting a regulator as in χ PT. Whereas any value of Λ is admissible in the power counting regime of χ PT (which is usually regarded to include the physical pion mass) in the two-channel HEFT case the regulator contains the physics necessary to describe the inelasticity. Moreover, if one wants the physics of the pion mass dependence to be contained within the Hamiltonian, one must use physically-motivated values to keep the errors corrected by the residual series expansion small.

With this new understanding, one should promote the regu-

lator parameter to a fit parameter to be constrained by experiment. This is explored in the next section.

E. Optimising Fit Parameters

In promoting the regulator parameters to fit parameters, one must acknowledge the correlation between Λ and the mass of the bare basis state, $m_\Delta^{(0)}$. For $\Lambda \sim 0.8$ GeV the correlation is strong as depicted in Figs. 6 and 13. To proceed, we refer to the single-channel fit parameters of Table I, Fit 1, where $\Lambda = 0.8$ GeV, and the fit was focused on the Δ resonance regime up to 1350 MeV. Here $m_\Delta^{(0)} = 1.36$ GeV and we use this as an initial anchor to remove the otherwise problematic $\Lambda \leftrightarrow m_\Delta^{(0)}$ correlations observed for $\Lambda < 2$ GeV.

For the optimal fit we allow the value of Λ at each interaction vertex to be a free parameter, constrained only by a lower

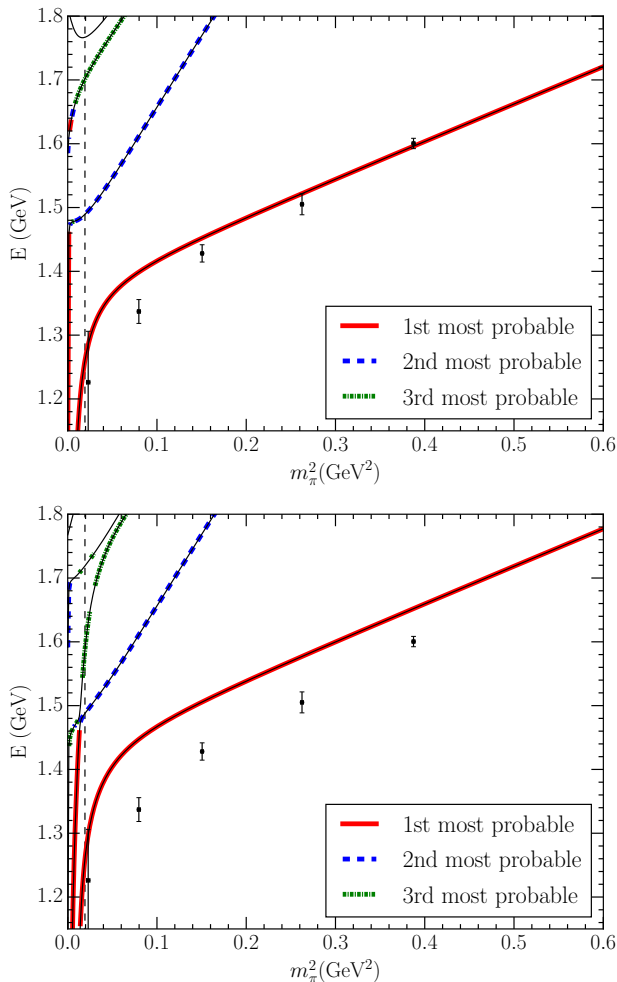


FIG. 15. Pion mass dependence of the finite-volume HEFT energy eigenvalues for $\Lambda = 0.8$ GeV (top) and $\Lambda = 1.2$ GeV (bottom) for the PACS-CS lattice length $L = 2.99$ fm. The vertical dashed (black) line denotes the physical pion mass. The thin diagonal (blue) dashed lines show the two-particle non-interacting energies and the thin horizontal (blue) line illustrates the bare basis state mass. The solid (black) points are the lowest lying Δ energies from lattice QCD [14]. The solid black curves illustrate the finite-volume energy levels predicted by HEFT from fits to experimental phase shifts and inelasticities. These lines are dressed by solid (red), dashed (blue) and dot-dashed (green) highlights indicating states with the largest, second-largest and third-largest contribution from the bare basis state $|\Delta_0\rangle$ respectively. As the PACS-CS results follow from local three-quark operators, they are expected to lie on a solid (red) energy eigenstate.

limit of 0.6 GeV in order to ensure valid low-energy physics is not unphysically suppressed. Here we label the regulator parameters in $G_{\pi N}^{\Delta}$ and $G_{\pi\Delta}^{\Delta}$ as $\Lambda_{\pi N}$ and $\Lambda_{\pi\Delta}$, respectively, while at each vertex in $V_{\pi B, \pi B'}$ we label the regulator parameters as $\Lambda_{v, \pi N}$ and $\Lambda_{v, \pi\Delta}$.

Initially fixing $m_{\Delta}^{(0)} = 1.36$ GeV, we are able to produce a fit which describes both the πN phase shift and the inelasticity. One can then examine the associated predictions for the quark mass dependence of the Δ spectrum and compare it with lattice QCD predictions. This comparison allows one

TABLE III. Two-channel fit parameters constrained to πN scattering data from Ref. [34]. Here, $m_{\Delta}^{(0)}$ is fixed to 1.34 GeV while all other parameters are optimised as described in the text.

Parameter	Fit VI
$m_{\Delta}^{(0)}/\text{GeV}$	1.340
$g_{\pi N}^{\Delta}$	0.1694
$g_{\pi\Delta}^{\Delta}$	0.0873
$v_{\pi N, \pi N}$	-0.0066
$v_{\pi N, \pi\Delta}$	-0.0433
$v_{\pi\Delta, \pi\Delta}$	-0.0390
$\Lambda_{\pi N}/\text{GeV}$	0.6686
$\Lambda_{\pi\Delta}/\text{GeV}$	0.7176
$\Lambda_{v, \pi N}/\text{GeV}$	0.6720
$\Lambda_{v, \pi\Delta}/\text{GeV}$	1.1991
α_0/GeV^{-1}	0.703
Pole 1 / GeV	$1.210 - 0.049i$
Pole 2 / GeV	$1.479 - 0.161i$

to fine tune the initial ansatz for the bare mass and improve agreement with the lattice results. This tuning process results in a bare mass of $m_{\Delta}^{(0)} = 1.34$ GeV, which simultaneously provides an excellent description of the P -wave πN scattering data and the finite volume lattice QCD results.

The final fit parameters are presented in Table III. We note that the optimal values for the regulator parameters are away from the lower limit of 0.6 GeV. The description of the πN phase shift and the inelasticity is presented in Fig. 16. Similarly to previous fits, this set of parameters produces a pole at the listed PDG position for the $\Delta(1232)$ of $1210 - 0.050i$ GeV. Unlike the previous case however, the second pole now falls within range of the PDG pole position for the $\Delta(1600)$, which is listed as approximately $(1.510 \pm 0.050) - (0.135 \pm 0.035)i$ GeV [35]. While it seems as though the introduction of the $\pi\Delta$ channel and the use of optimised regulator parameters is able to shift the second pole position to be inline with that of the $\Delta(1600)$, this is outside the scope of this study though it is a promising direction for further research.

The associated prediction for the quark mass dependence of this fit is presented in Fig. 17. This fit provides a good description of the lattice QCD results from PACS-CS [14]. The second lightest lattice point is within $\sim 2\sigma$ of the lattice QCD point, and is expected to rise in a higher-statistics analysis. Here, a new slope for the quark-mass dependence of the bass mass which best describes the lattice QCD data is found. This takes a value of $\alpha_0 = 0.703$ GeV^{-1} , and the χ^2/dof for this one parameter fit is 0.89. In Fig. 18, it can be seen how the composition of the ground state varies as the pion mass increases. This shows how even before reaching the physical point, the ground state is heavily dominated by the bare basis state contribution. Indeed, for $m_{\pi}^2 \gtrsim 0.1$ GeV^2 , the ground state is almost completely described by a simple three-quark

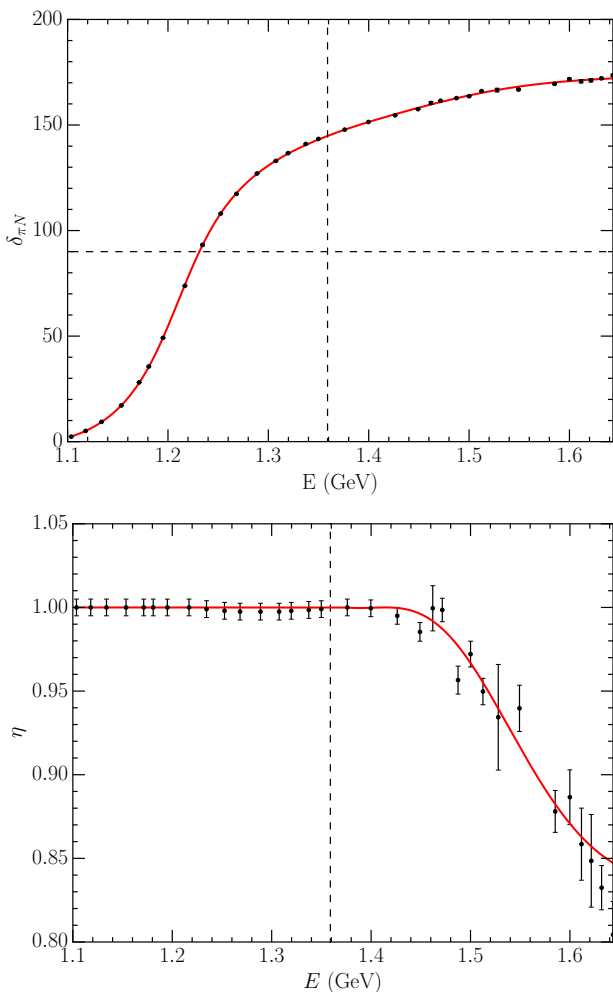


FIG. 16. P -wave πN phase shift and inelasticity from the fit with optimised regulator parameters as described in the text, where the vertical dashed (black) line shows the $\pi\Delta$ threshold. The optimised parameters for these results are contained in Table III.

like bare state, as is predicted by the linearity of the PACS-CS data.

Similarly we also present the final predictions for the lattice size L dependence of the eigenstates. The finite-volume energy spectrum in L is given in Fig. 19, though as expected this takes a near-identical form to the spectra generated by previous fits. Here, it is satisfying to see that the location of the state with the largest bare component, shown with red highlighting, remains around the location of the physical Δ mass of 1232 MeV. This is manifest through transitions to the first excited state at ~ 5.5 fm, and to the second excited state at ~ 7.5 fm. This becomes especially clear in Fig. 20, where the L -dependence of the ground state and first excited-state eigenvectors are shown. Here, it is made clear how as L increases, the ground state changes from being almost completely dominated by the bare basis state, to a state composed almost entirely of the $\pi N(k=1)$ basis state. The first excited state undergoes a similar metamorphosis, changing from a state mostly described by $\pi N(k=1)$ contributions, to being

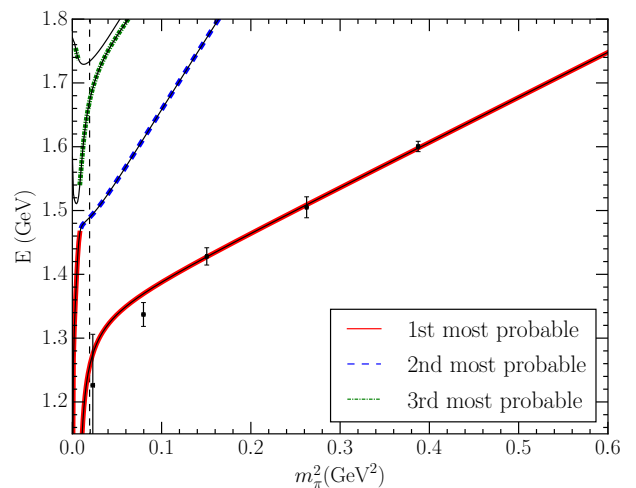


FIG. 17. Pion mass dependence of the finite-volume HEFT eigenvalues for $L = 2.99$ fm, allowing all regulator parameters to be optimised with the couplings. Optimised values are presented in Table III. The vertical dashed (black) line denotes the physical pion mass. The solid (black) points are the lowest lying Δ energies from lattice QCD [14]. The solid black curves illustrate the finite-volume energy levels predicted by HEFT from a fit to the experimental phase shifts and inelasticities as illustrated in Fig. 16. These lines are dressed by solid (red), dashed (blue) and dot-dashed (green) highlights indicating states with the largest, second-largest and third-largest contribution from the bare basis state $|\Delta_0\rangle$ respectively. As the PACS-CS results follow from local three-quark operators, they are expected to lie on a solid (red) energy eigenstate.

composed primarily of $\pi N(k=2)$. These two figures serve to demonstrate how the contributions from the bare basis state move throughout the eigenstates, producing the transitions in the red line shown in Fig. 19.

VI. CONCLUSION

We have examined the process of renormalisation in non-perturbative Hamiltonian Effective Field Theory (HEFT). As an extension of effective field theory, HEFT provides a bridge between the infinite-volume scattering data of experiment and the finite-volume spectrum of energy eigenstates in lattice QCD. Our question has been, to what extent do the celebrated features of finite-range regularisation survive in HEFT.

HEFT brings the insight of experimental data to the finite-volume of the lattice through the parametrisation of a Hamiltonian built on a basis of non-interacting multiparticle states. Through a process of constraining Hamiltonian parameters to scattering data, and then solving for the eigenmodes of a finite-volume matrix Hamiltonian, one obtains finite-volume energy eigenvalues and eigenvectors describing the composition of the finite volume states. A key question is to ascertain the regularisation-scheme dependence of these eigenvectors.

Using the FRR scheme, an expression for the S -matrix was obtained by solving the coupled-channel, Bethe-Salpeter equations, and the phase shifts and inelasticities for the system

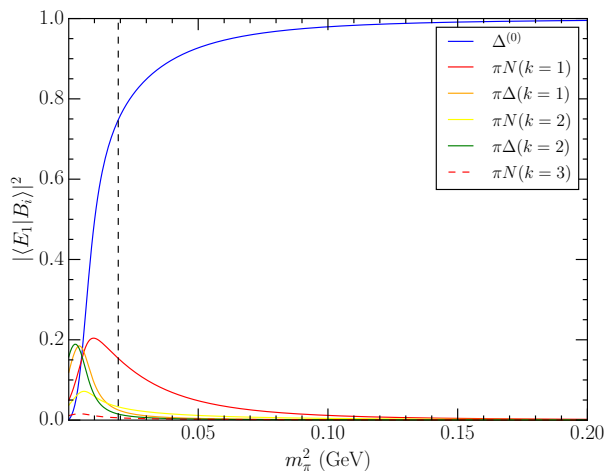


FIG. 18. Pion mass dependence of the eigenvector describing the composition of the lowest lying energy in the two-channel case with πN and $\pi\Delta$ scattering channels, using the optimised fit parameters. The dashed vertical line represents the physical pion mass.

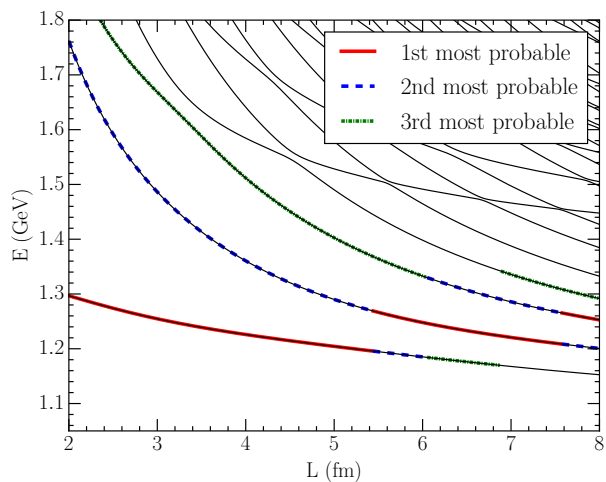


FIG. 19. Lattice volume dependence of the finite-volume HEFT eigenvalues for a physical pion mass, and optimised fit parameters given in Table III. The solid (red), dashed (blue) and dot-dashed (green) highlights on the eigenvalues correspond to the states with the largest, second-largest and third-largest contribution from the bare basis state $|\Delta_0\rangle$ respectively.

were then extracted. These quantities were fit to the SAID Partial-Wave Analysis Facility experimental scattering data [34] by adjusting the parameters of the Hamiltonian. These optimised parameters then serve as inputs for a Hamiltonian matrix model. By solving the eigenvalue equation for this Hamiltonian the finite-volume energy eigenvalues and eigenvectors describing the composition of the finite volume states were resolved.

We considered the P -wave, $I(J^P) = \frac{3}{2}(\frac{3}{2}^+)$ Δ resonance channel. A simple description of the Δ is to consider only the mixing of a bare Δ with a two-particle πN state. Considering a basic system such as this allowed for the development

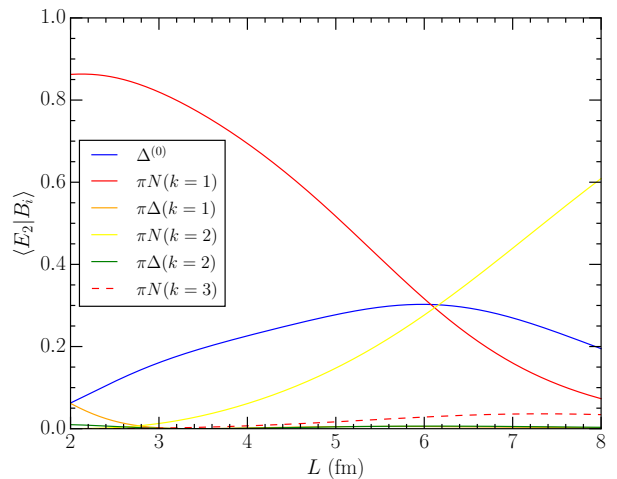
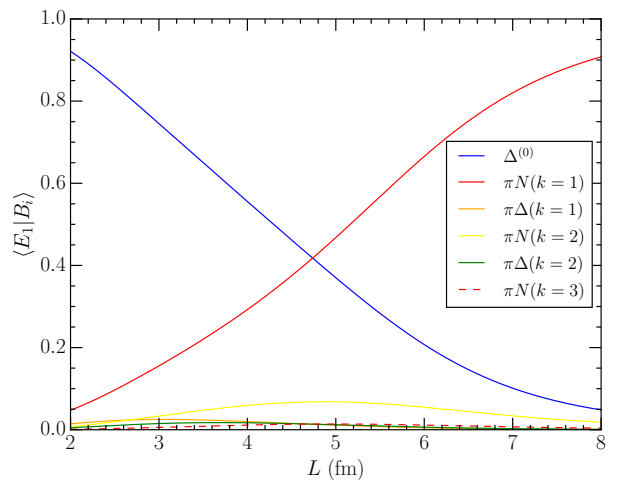


FIG. 20. Lattice size dependence of the eigenvectors describing the composition of the ground state (upper) and the first excited state (lower) in the two-channel case with πN and $\pi\Delta$ scattering channels, using the optimised fit parameters.

of intuition into the results of HEFT, before moving onto the more complicated two-channel system. By considering values for the regulator parameter ranging from $\Lambda = 0.8$ GeV to $\Lambda = 8.0$ GeV, we were able to fit the scattering data to varying degrees of success. These fits produced a pole in agreement with the value listed by the Particle Data Group. By solving the Hamiltonian matrix for this system at varying lattice sizes L , a finite-volume energy spectrum was found.

While the eigenvalues of the matrix Hamiltonian constrained to experimental scattering data do not depend on the regulator parameter Λ , the eigenvectors of the Hamiltonian do show a significant dependence on Λ . As Λ increases and short-distance interactions are allowed between the effective fields, the bare basis state contribution to low-lying finite-volume states decreases, implying that a bare basis state may not be necessary for a description of the Δ resonance. To resolve the validity of this conjecture, the pion mass dependence of the HEFTs was examined.

Extending HEFT beyond the physical pion mass allows for

a direct comparison to lattice QCD calculations available at many pion masses. In performing this comparison, it became clear that as Λ becomes large, short-distance errors are made in the Hamiltonian interactions and these errors require large contributions from the residual series expansion terms contained within the mass function of the bare basis state. Large Λ values are incompatible with the simple linear quark-mass dependence of the bare-state mass, which is predicted in quark models.

For large Λ the physics is no longer contained within the interactions of the Hamiltonian alone. Rather an elaborate residual series expansion is required to address the short-distance errors made in the unphysically hard interactions included in the Hamiltonian. Moreover, the eigenvectors of the Hamiltonian formulated with large Λ will reflect the erroneous incorporation of short-distance interactions.

In summary, the composition of the eigenstates contained within the eigenvectors of HEFT have physical relevance only when a simple ansatz for the quark-mass dependence of the bare mass (the residual series expansion) is sufficient to describe results from lattice QCD. In this case, the correct physics is contained within the interactions of the Hamiltonian and physical insight can flow from the eigenvectors. Indeed the regulator dependence of the eigenvectors for $\Lambda \sim 0.8$ GeV is small.

Having gained intuition into the structure of the Δ in the simple single-channel case, the more complicated two-channel system was considered, allowing the scattering data to be described at higher energies and introducing an inelasticity for consideration. While the scattering phase shifts could be described for various values of Λ , an accurate description of the inelasticity required a value of Λ consistent with phenomenologically motivated values associated with the induced pseudoscalar form factor of a baryon.

Thus consideration of the two-channel case has made it clear that nonperturbative HEFT does not enjoy the same freedom in selecting a regulator as in χ PT. Whereas any value of Λ is admissible in the power counting regime of χ PT (which is usually regarded to include the physical pion mass) in the two-channel HEFT case the regulator contains the physics necessary to describe the inelasticity. Λ must take physically motivated values to enable a description of the inelasticity.

Moreover, by considering the pion mass dependence of the spectra generated by different regulator parameters, and comparing them to lattice QCD results, the same issues discovered in the single channel case were observed. A simple ansatz for the bare-state quark-mass dependence, demands the selection of physically-motivated regulator parameters to keep the short-distance errors small and thus the residual series expansion terms small. With the correct physics contained within the Hamiltonian, the eigenvectors of the Hamiltonian provide physically relevant insight into the composition of the finite-volume energy eigenstates.

With this new understanding, the regulator parameters of the meson-baryon interaction channels were promoted to fit parameters to be constrained by both experimental scattering data and lattice QCD results. The final fits provide good descriptions of the phase shift, inelasticity and current lattice

QCD energies and provide predictions for the Δ spectrum to be observed in future lattice QCD calculations at a variety of quark masses.

Future work should consider the effects of moving frames on the Δ system in HEFT [40] in order to compare with recent lattice QCD results [15]. Additionally, the understanding of the roles of the bare mass and regulator parameters will prove useful for the study of new areas of interest such as the odd-parity nucleon resonances, where recent research [41] has indicated that two bare states may be required to adequately describe the system.

ACKNOWLEDGEMENTS

DBL thanks Albert Kong for discussions in the early phase of this research. This research was supported by the Australian Government Research Training Program Scholarship, and with supercomputing resources provided by the Phoenix HPC service at the University of Adelaide. This research was undertaken with the assistance of resources from the National Computational Infrastructure (NCI), provided through the National Computational Merit Allocation Scheme, and supported by the Australian Government through Grant No. LE190100021 and the University of Adelaide Partner Share. This research was supported by the Australian Research Council through ARC Discovery Project Grants Nos. DP180100497 (A.W.T.) and DP190102215 and DP210103706 (D.B.L.). J.-J. Wu was supported by the Fundamental Research Funds for the Central Universities, by the National Key R&D Program of China under Contract No. 2020YFA0406400, and by the Key Research Program of the Chinese Academy of Sciences, Grant NO. XDPB15.

- [1] M. Lüscher. Volume dependence of the energy spectrum in massive quantum field theories I. Stable particle states. *Communications in Mathematical Physics*, 104(2):177–206, June 1986.
- [2] M. Lüscher. Volume dependence of the energy spectrum in massive quantum field theories II. Scattering states. *Communications in Mathematical Physics*, 105(2):153–188, June 1986.
- [3] Martin Lüscher. Two-particle states on a torus and their relation to the scattering matrix. *Nuclear Physics B*, 354(2):531–578, May 1991.
- [4] Song He, Xu Feng, and Chuan Liu. Two particle states and the S-matrix elements in multi-channel scattering. *JHEP*, 07:011, 2005.
- [5] Michael Lage, Ulf-G. Meissner, and Akaki Rusetsky. A Method to measure the antikaon-nucleon scattering length in lattice QCD. *Physics Letters*, B681:439–443, 2009.
- [6] V. Bernard, M. Lage, U. G. Meissner, and A. Rusetsky. Scalar mesons in a finite volume. *JHEP*, 01:019, 2011.
- [7] Peng Guo, Jozef Dudek, Robert Edwards, and Adam P. Szczepaniak. Coupled-channel scattering on a torus. *Physical Review*, D88(1):014501, 2013.
- [8] B. Hu, R. Molina, M. Döring, and A. Alexandru. Two-flavor Simulations of the $\rho(770)$ and the Role of the $\bar{K}K$ Channel. *Physical Review Letters*, 117(12):122001, September 2016.
- [9] Ning Li and Chuan Liu. Generalized Lüscher Formula in Multi-channel Baryon-Meson Scattering. *Physical Review D*, 87(1):014502, January 2013.
- [10] Maxwell T. Hansen and Stephen R. Sharpe. Multiple-channel generalization of Lellouch-Lüscher formula. *PoS, LATTICE2012*:127, 2012.
- [11] M. Döring, H.-W. Hammer, M. Mai, J.-Y. Pang, A. Rusetsky, and J. Wu. Three-body spectrum in a finite volume: The role of cubic symmetry. *Physical Review D*, 97(11):114508, June 2018.
- [12] Maxwell T. Hansen and Stephen R. Sharpe. Lattice QCD and Three-particle Decays of Resonances. *Annual Review of Nuclear and Particle Science*, 69(1):65–107, October 2019.
- [13] Tyler D. Blanton, Fernando Romero-López, and Stephen R. Sharpe. $I = 3$ three-pion scattering amplitude from lattice QCD. *Physical Review Letters*, 124(3):032001, January 2020.
- [14] S. Aoki et al. 2+1 Flavor Lattice QCD toward the Physical Point. *Phys. Rev. D*, 79:034503, 2009.
- [15] Christian Walther Andersen, John Bulava, Ben Hörz, and Colin Morningstar. Elastic $I = 3/2$ p -wave nucleon-pion scattering amplitude and the $\Delta(1232)$ resonance from $N_f=2+1$ lattice QCD. *Phys. Rev.*, D97(1):014506, 2018.
- [16] Giorgio Silvi et al. P -wave nucleon-pion scattering amplitude in the $\Delta(1232)$ channel from lattice QCD. *Phys. Rev. D*, 103(9):094508, 2021.
- [17] J. M. M. Hall, A. C.-P. Hsu, D. B. Leinweber, A. W. Thomas, and R. D. Young. Finite-volume matrix hamiltonian model for a $\Delta \rightarrow N\pi$ system. *Phys. Rev. D*, 87:094510, May 2013.
- [18] Jia-Jun Wu, T.-S. H. Lee, A. W. Thomas, and R. D. Young. Finite-volume Hamiltonian method for coupled channel interactions in lattice QCD. *Physical Review C*, 90(5):055206, November 2014.
- [19] Ross Daniel Young, Derek Bruce Leinweber, and Anthony William Thomas. Convergence of chiral effective field theory. *Prog. Part. Nucl. Phys.*, 50:399–417, 2003.
- [20] Derek Bruce Leinweber, Anthony William Thomas, and Ross Daniel Young. Physical nucleon properties from lattice QCD. *Phys. Rev. Lett.*, 92:242002, 2004.
- [21] Derek Bruce Leinweber, Anthony William Thomas, and Ross Daniel Young. Power counting regime of chiral extrapolation and beyond. *PoS, LAT2005*:048, 2006.
- [22] Murray Gell-Mann, R. J. Oakes, and B. Renner. Behavior of current divergences under $SU(3) \times SU(3)$. *Phys. Rev.*, 175:2195–2199, 1968.
- [23] Derek Bruce Leinweber, Anthony William Thomas, Kazuo Tsushima, and Stewart Victor Wright. Baryon masses from lattice QCD: Beyond the perturbative chiral regime. *Phys. Rev. D*, 61:074502, 2000.
- [24] J. M. M. Hall, D. B. Leinweber, and R. D. Young. Power Counting Regime of Chiral Effective Field Theory and Beyond. *Phys. Rev. D*, 82:034010, 2010.
- [25] J.M.M. Hall, F.X. Lee, D.B. Leinweber, K.F. Liu, N. Mathur, R.D. Young, and J.B. Zhang. Chiral extrapolation beyond the power-counting regime. *Phys. Rev. D*, 84:114011, 2011.
- [26] J.M.M. Hall, D.B. Leinweber, and R.D. Young. Chiral extrapolations for nucleon magnetic moments. *Phys. Rev. D*, 85:094502, 2012.
- [27] J.M.M. Hall, D.B. Leinweber, and R.D. Young. Chiral extrapolations for nucleon electric charge radii. *Phys. Rev. D*, 88(1):014504, 2013.
- [28] P.A.M. Guichon, G.A. Miller, and A.W. Thomas. The axial form factor of the nucleon and the pion-nucleon vertex function. *Physics Letters B*, 124(1):109–112, 1983.
- [29] Anthony William Thomas. Chiral Symmetry and the Bag Model: A New Starting Point for Nuclear Physics. *Adv. Nucl. Phys.*, 13:1–137, 1984.
- [30] Gerald A. Miller, Anthony William Thomas, and S. Theberge. Pionic Corrections in the MIT Bag Model. *Comments Nucl. Part. Phys.*, 10(3):101–108, 1981.
- [31] Yan Li, Jia-Jun Wu, Curtis D. Abell, Derek B. Leinweber, and Anthony W. Thomas. Partial Wave Mixing in Hamiltonian Effective Field Theory. *Phys. Rev. D*, 101(11):114501, 2020.
- [32] Zhan-Wei Liu, Waseem Kamleh, Derek B. Leinweber, Finn M. Stokes, Anthony W. Thomas, and Jia-Jun Wu. Hamiltonian effective field theory study of the $\mathbf{N}^*(1535)$ resonance in lattice QCD. *Physical Review Letters*, 116(8):082004, February 2016.
- [33] Richard A. Arndt, John M. Ford, and L. David Roper. PION - NUCLEON PARTIAL WAVE ANALYSIS TO 1100-MeV. *Phys. Rev. D*, 32:1085, 1985.
- [34] INS Data Analysis Center. <http://gwdac.phys.gwu.edu/>. Online.
- [35] Particle Data Group. Review of Particle Physics*. *Progress of Theoretical and Experimental Physics*, 2020(8), 08 2020. 083C01.
- [36] Gerald A. Miller, Anthony William Thomas, and S. Theberge. Pion - Nucleon Scattering in the Cloudy Bag Model. *Phys. Lett. B*, 91:192–195, 1980.
- [37] S. Theberge, Anthony William Thomas, and Gerald A. Miller. The Cloudy Bag Model. 1. The $(3,3)$ Resonance. *Phys. Rev. D*, 22:2838, 1980. [Erratum: *Phys.Rev.D* 23, 2106 (1981)].
- [38] Judith A. McGovern and Michael C. Birse. On the absence of fifth order contributions to the nucleon mass in heavy baryon chiral perturbation theory. *Phys. Lett. B*, 446:300–305, 1999.
- [39] Ross Daniel Young, Derek Bruce Leinweber, and Anthony William Thomas. Leading quenching effects in the pro-

- ton magnetic moment. *Phys. Rev. D*, 71:014001, 2005.
- [40] Yan Li, Jia-jun Wu, Derek B. Leinweber, and Anthony W. Thomas. Hamiltonian effective field theory in elongated or moving finite volume. *Phys. Rev. D*, 103(9):094518, 2021.
- [41] Finn M. Stokes, Waseem Kamleh, and Derek B. Leinweber. Elastic Form Factors of Nucleon Excitations in Lattice QCD. *Phys. Rev. D*, 102(1):014507, 2020.